This chapter is mainly focused on metal phosphonate (Ce-ATMP) through the sol-gel process which may be used to sorbent for removal of transition and heavy metal ions. It's characterized via using techniques including FTIR, SEM-EDX, XRD and TGA.

5.1. Introduction

Poor quality of water is an ongoing issue caused by water pollution. Sedimentary materials and potentially hazardous metals such as specific metal ions are identified contaminants found in waste water [1,2]. Heavy metal species such as Pb^{2+}, Cu^{2+}, Cd^{2+}, Hg^{2+} and Ni^{2+} ions are common pollutants introduced into natural water from variety of industrial effluents. Since, heavy metal-laden effluents are being released by the various industrial sources [3,4]. The human health is adversely affected by such toxic metals through detrimental the brain, kidneys, reproductive and cardiovascular systems [5-7]. To find solution of above problem, numerous materials, methods and technologies have been developed over the period of time for the effective removal of toxic heavy metals from the aqueous bodies [3]. Various strategies are in use to irradicate the source of contamination [8,9]. Among them ion exchange reported to be technically simple potential for a wide spectrum of metal ions [10]. Recently, the applicability of ion-exchangers has been remarkably enhanced by the preparation of new organic-inorganic hybrid ion-exchangers this is because of the compatible properties of organic and inorganic constituents which make the process efficient and specific [11,12]. Over the past few years, a large number of such hybrid ion-exchangers have been synthesized and their potential is analyzed [13-16].

Phosphoric acids are well known for their interactions with metal ions. In view of such potent materials, metal phosphonates (tetravalent metal acid (TMA) salts) are obtained as hybrid porous materials with strong inorganic backbones containing both organic and inorganic properties. Interestingly, they possess good affinity for metal ions high water-content, mechanical, chemical and thermal stabilities. In this context, phosphonates of tetravalent metals are now extensively used as exchanger material [17-20]. The efficiency of donor groups in the tetravalent metal ion bonding by claw-type amino phosphonic acids has garnered a lot of interest owing to its binding ability [21,22]. The literature reports show that studies on phosphonates of Zr^{4+} and Ti^{4+}, with different phosphonic acids, are well established, in an ion exchange process [23-27].

In this regard, herein, we report the systematic study of microporous cerium-based organic-inorganic hybrid material (using amino tris-(methylene phosphonic acid)) as a phosphonic acid (ATMP) [23]. In contrast to phosphoric acid (H_3PO_4) which has three structural hydroxyl (-OH) groups, ATMP has six and therefore, resulting cerium phosphonate (Ce-ATMP) with improved a cation-exchange capacity (in terms of pendant hydroxyl (-OH) groups).

Here, Ce-ATMP has been synthesized using sol-gel route [19,23] and characterized by different analytical techniques including ICP-AES, CHN, FTIR, TGA, XRD, FESEM, EDX analysis. Characteristics of physical and ion-exchange have also been studied. Thus, it was aim to apply a potential of the cation exchanger Ce-ATMP. By assessing the distribution coefficient (K_d) values in aqueous as well as various electrolyte media/concentrations and breakthrough capacity (BTC), the sorption behavior among the metal ions under research towards Ce-ATMP has been explored. Langmuir adsorption isotherms have been used to study the adsorption of metal ions at various temperatures between 300 and 333 K at 10 K intervals. Evaluations have also been done on thermodynamic parameters including equilibrium constant (K), Gibbs free energy change, enthalpy change, entropy change and with the help of pseudo-first-order, pseudo-second-order and intra-particle diffusion calculations, Ce-ATMP has been utilized to examine the kinetic order of transition metal ions (Cu^{2+}, Ni^{2+}, Co^{2+}, Zn^{2+}), as well as heavy metal ions (Pb^{2+}, Cd^{2+}, Hg^{2+}). These metal ions' elution behavior has been investigated using acids and electrolytes (HNO_3, $HClO_4$, NH_4NO_3, and CH_3COOH). Depending on the separation factor, a few efficient binary and ternary metal ion separations have been performed.

5.2. Experimental section

All the chemical materials, methods and physical measurements utilized in this work are comprehensively interpreted in the “Chapter 2” (Section 2.1, 2.2 and 2.3).

5.2.1. Distribution coefficient (K_d) study using Ce-ATMP

Distribution coefficient (K_d) studies for transition and heavy metal ions (Co^{2+}, Ni^{2+}, Cu^{2+}, and Zn^{2+}, Cd^{2+}, Hg^{2+}, and Pb^{2+}) were evaluating using batch method were as described earlier in Chapter 3 (Sec. 3.2.1).

5.2.2. Breakthrough capacity (BTC)

Relating the BTC evaluations, 0.5 g of the ion exchanger Ce-ATMP was placed in a glass column (30 cm × 1 cm) and attentively washed with DI water, and the flow rate was adjusted to 0.5 mL·min^{-1}. Metal ion concentration was established quantitatively by EDTA titration [23]. For Breakthrough capacity, 5 mL fractions of each individual metal ion (transition metal ions Co^{2+}, Ni^{2+}, Cu^{2+}, and Zn^{2+} and heavy metal ions Pb^{2+}, Cd^{2+}, and Hg^{2+}) at a concentration of 0.002 M was passed through the column, and the effluent was collected until the metal-ion concentrations in the feed and effluent were the equitable. Plotting the ratio C_e/C_0 versus the effluent volume provided the breakthrough curve, where C_0 and C_e are the concentrations of the initial solution and the effluent, respectively. BTC was calculated as (Equation 1):

$$BTC = \frac{C_0 V_{10\%}}{W} \quad (1)$$

where W is the exchanger's weight (mg), C_0 is the metal ion's initial concentration (mol.L^{-1}), and $V_{10\%}$ is the volume (mL) of metal-ion solution that had flowed through the column when the exit concentration achieved 10% of the initial concentration.

5.2.3. Adsorption studies

Effect of pH, contact time and temperature on adsorption/ion exchange were determined using batch technique as specified earlier in “Chapter 3” (Sec. 3.2.2. and 3.2.2.1).

5.2.4. Thermodynamic studies

5.2.4.1. Equilibrium time determination

These investigations involved shaking 0.1 g of exchanger Ce-ATMP (in H^+ form) with 0.002 M metal ion solution in a stoppered conical flask for durations that varied from 10 to 80 min were as described earlier in “Chapter 3” (Sec. 3.2.3.1).

5.2.4.2. Equilibrium experiments

These investigations were as described earlier in “Chapter 3” (Sec. 3.2.3.2).

5.2.5. Kinetic studies

The efficiency of an ion exchanger is mostly determined by the reaction kinetics. The commonly-used pseudo-first-order, pseudo-second-order, and intra-particle diffusion kinetic

models were applied to investigate the rate-determining step for ion exchange, discussed earlier in "Chapter 3" (Sec. 3.2.4, 3.2.4.1, 3.2.4.2 and 3.2.4.3).

5.2.6. Elution Studies

The column was set up for single metal elution investigations as described earlier in "Chapter 3" (Sec. 3.2.1.5).

5.2.7. Studies on binary and ternary separation

The metal ion mixture (0.002 M, 10 mL for each metal ion) must be separated into binary or ternary separations was loaded onto the column. Passing the appropriate eluants through the column helped to accomplish the separations. The eluant was chosen for a particular metal ion pair based on the K_d values of the respective metal ions (in a certain medium) in which the separation factor was largest. Using EDTA titration, metal ion concentrations were quantitatively ascertained [20,28,29]. For each metal ion that was eluted, the amount (E, %) was calculated using a similar equation that was utilized for the individual metal investigations.

5.2.8. Regeneration and reusability studies of Ce-ATMP

The batch technique was used to evaluate the Ce-ATMP ion exchanger's regeneration and reuse in the instance of copper ions. In this instance, 0.1 g of Ce-ATMP had been mixed to a Cu^{2+} solution at the ideal concentration (0.002 M) for 60 min (the maximum equilibrium time), following which the metal ion concentration was assessed by EDTA titration and the K_d value was established. 50 mL of HNO_3 (1 M) was utilized to treat the Cu^{2+}-exchanged Ce-ATMP for 30 min while shaking it occasionally. The acid was then removed from the Ce-ATMP sample by decantation, and any remaining acid was washed away with DIW, For the exchanger to be completely free of Cu^{2+}, this procedure was performed at minimum five times. This regenerated Ce-ATMP was employed to ascertain K_d values. This process was repeated until wide variations in K_d values were observed. In each consecutive cycle, $K_{d(R)}$, the percentage retention of K_d value, was computed as follows (Equation 9):

$$K_{d(R)} = \left[\frac{K_{d(C)}}{K_d}\right] \times 100 \quad (2)$$

Where, K_d denotes the value gained at the initial stage and $K_{d(C)}$ denotes the value acquired during that cycle [23].

5.3. Result and discussion

5.3.1. Physico-chemical and ion-exchange characteristics

Physico-chemical and ion-exchange characteristics of the prepared Ce-ATMP have been illustrated in **Table 5.1**. pH titration curve as weak cation exchanger depicted in **Figure 5.1**. Cerium phosphonate was observed yellow floppy granules as physical appearance. The Na^+ cation exchange capacity (CEC) ascertained through the column method at room temperature was 2.40 mequiv·g^{-1} **(Figures 5.2 (a) and (b))**. This implies that 0.5 M is the minimum molar concentration and 200 mL is the optimal volume of sodium acetate solution for maximum elution of H^+ ions from 0.5 g of the cation exchanger. The calcination investigation (impact of heating to 500 °C within a 100 °C interval) demonstrates that the existence of protonic sites is represented by the condensation of -OH groups, which indicates the elimination of hydrated water, and a progressive decrease in CEC values with heating **(Table 5.1)**.

Table 5.1. Physico-chemical and Ion exchange Characteristics for Ce-ATMP.

Physico-chemical characteristics	
Physical Appearance	Yellow floppy granules
Particle size	0.39 - 0.65 mm
% Moisture content	8.71 %
True density	1.3 g·mL^{-1}
Apparent density	0.76 g·mL^{-1}
Chemical Stability	
Acids	3 N H_2SO_4, 5 N HNO_3, 5 N HCl
Bases	0.5 N NaOH, 0.5 N KOH
Organic Solvents	Ethanol, Acetone, Acetic Acid, Toluene
Ion Exchange characteristics	
Void volume fraction	0.42
Concentration of fixed ionogenic group	2.61 mmol·g^{-1}
Volume capacity	1.51 meq·mL^{-1}
Nature of exchanger	Weak cation Exchanger
Cation exchange capacity (CEC) (mequiv·g^{-1})	
Temperature (°C)	CEC (mequiv·g^{-1})
Room Temperature (~28±2 °C)	2.20
100	2.00
200	1.84
300	1.48
400	1.00
500	0.80

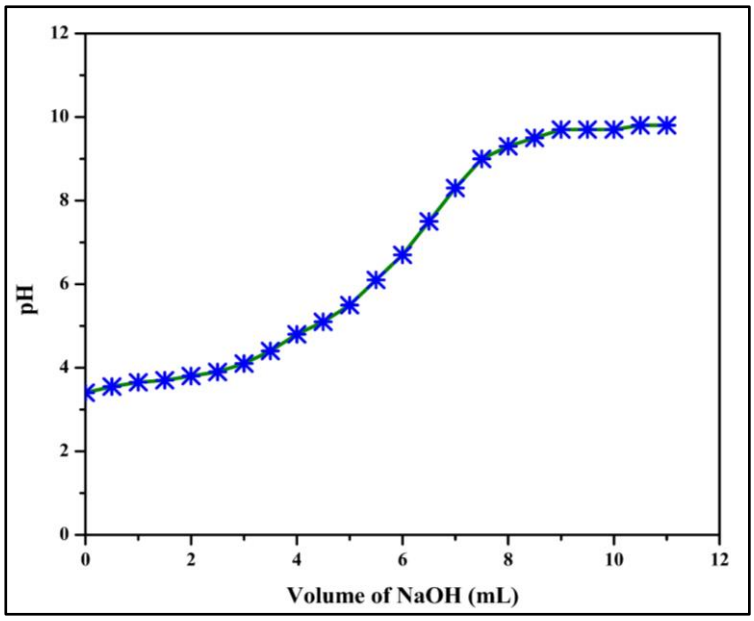

Figure 5.1. pH titration curve of Ce-ATMP.

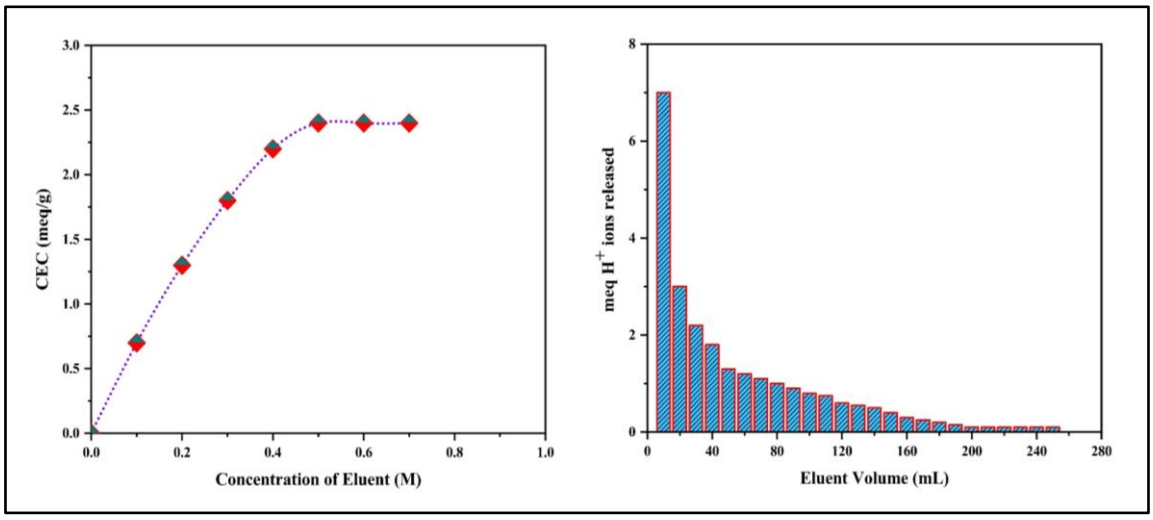

Figure 5.2. (a) Concentration and (b) Volume optimization for determination of CEC using Ce-ATMP.

5.3.2. Elemental analysis (ICP-AES and CHN analysis)

ICP-AES results for Ce-ATMP are as follows: % Ce = 30.89 and % P = 16.20. From the CHN analysis data, % C = 6.33, % H = 2.952, % N = 2.41. The observed C, H, N analysis data and theoretical values can be correlated. Based on the ICP-AES, CHN data, Ce-ATMP is formulated as $Ce(C_3H_{12}N_1P_3O_9)\cdot 4H_2O$ [19].

5.3.3. FESEM-EDS

SEM images of Ce-ATMP and metal loaded Ce-ATMP show an irregular morphology. **(Figures 5.3)**. EDX graphs are in conformity with the obtained elemental analysis of Ce-ATMP and metal loaded Ce-ATMP as seen in **(Figure 5.4 and Figure 5.5)**.

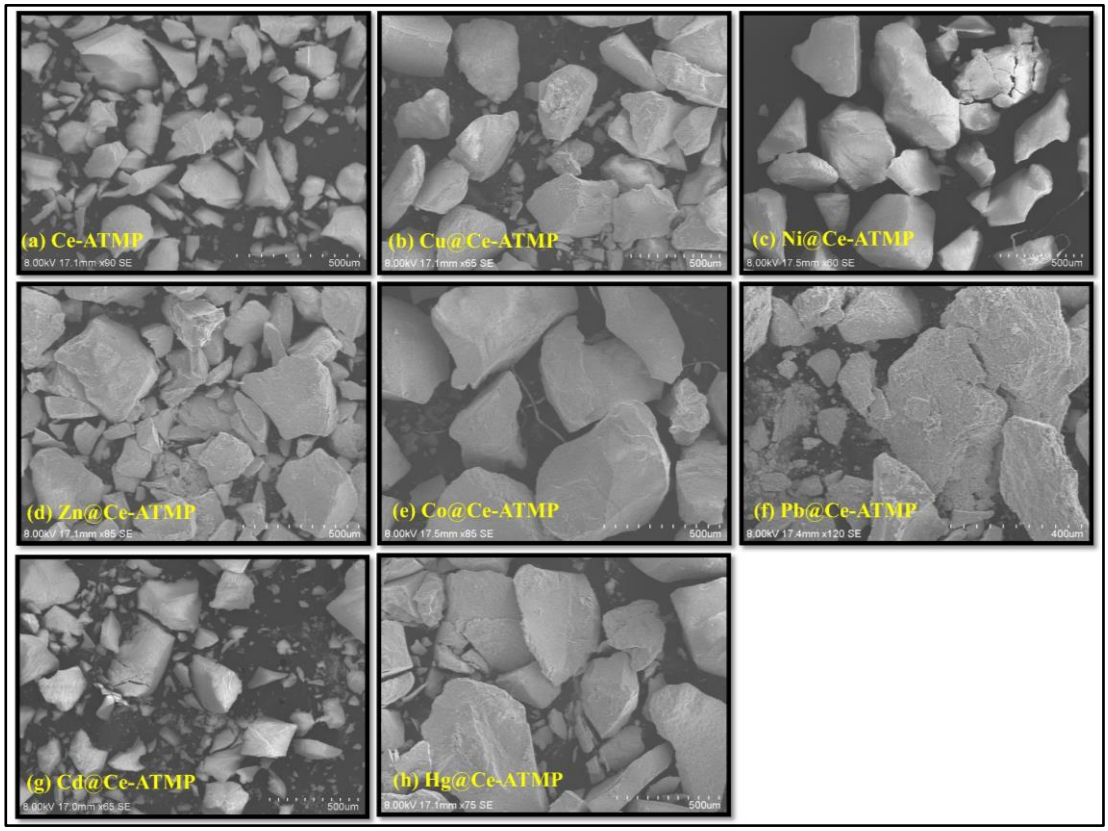

Figure 5.3. SEM images of (a) Ce-ATMP (b) Cu@Ce-ATMP (c) Ni@Ce-ATMP (d) Zn@Ce-ATMP (e) Co@Ce-ATMP (f) Pb@Ce-ATMP (g) Cd@Ce-ATMP and (h) Hg@Ce-ATMP.

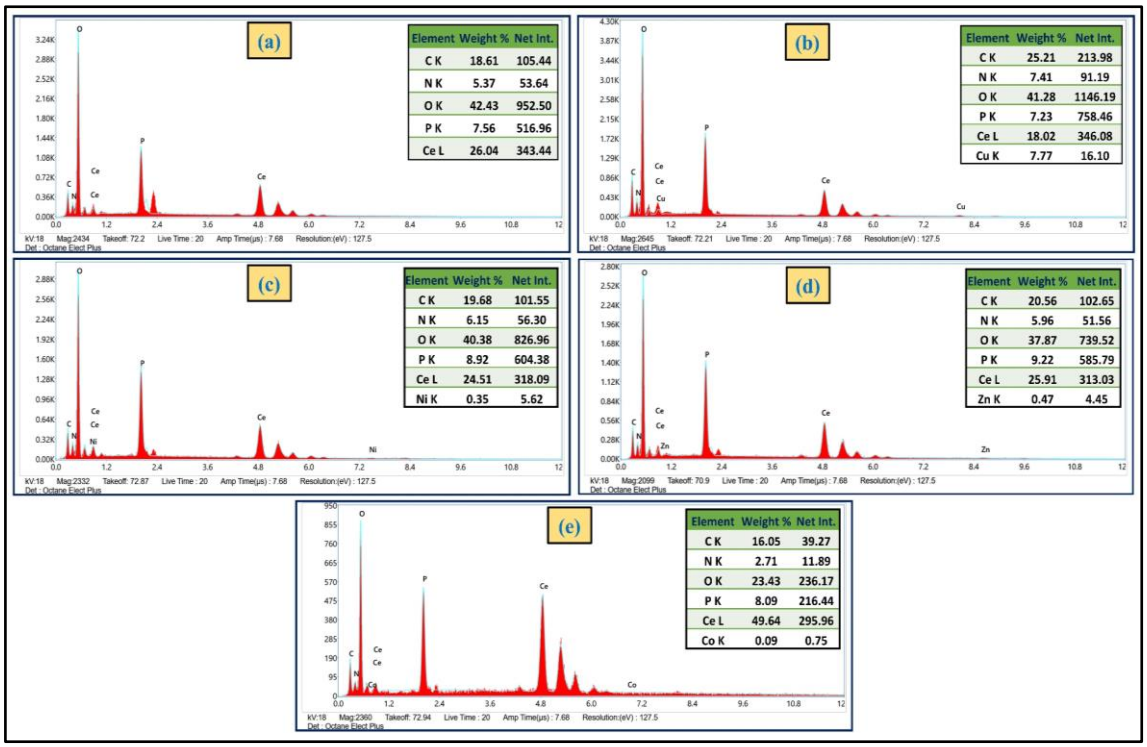

Figure 5.4. EDX spectra of (a) Ce-ATMP and Transition metal ion (b) [Cu@Ce-ATMP] (c) [Ni@Ce-ATMP] (d) [Zn@Ce-ATMP] (e) [Co@Ce-ATMP].

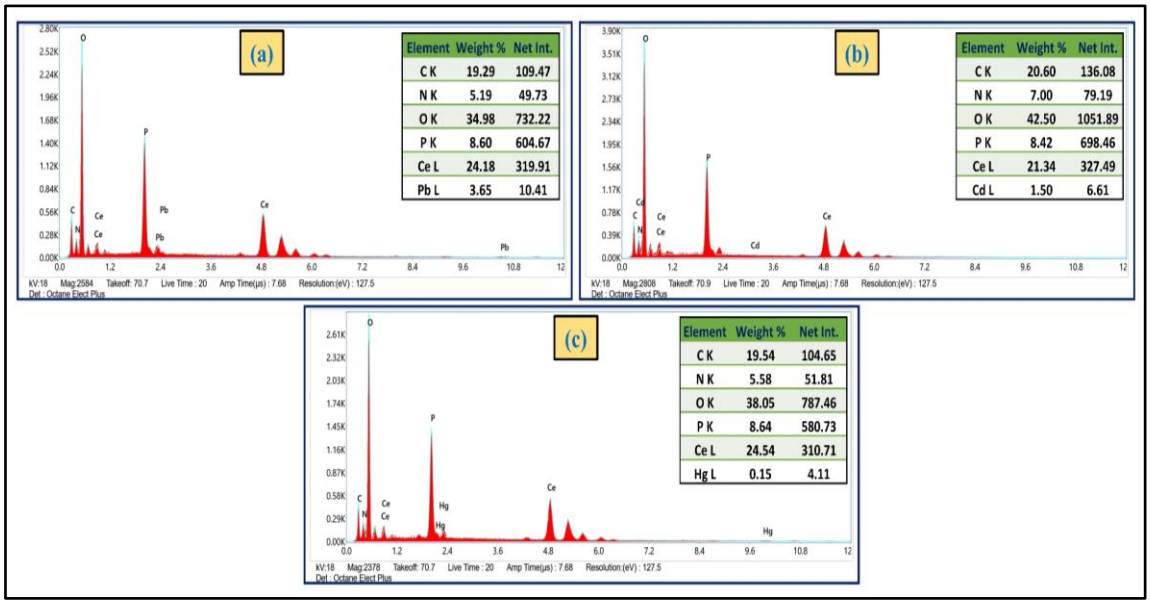

Figure 5.5. EDX spectra of heavy metal ion (a) [Pb@Ce-ATMP] (b) [Cd@Ce-ATMP] and (c) [Cu@Ce-ATMP].

5.3.4. TGA

TGA of Ce-ATMP **(Figure 5.6)** illustrates two major weight loss regions, where the loss of moisture/hydrated water occurs up to ~120 °C and in the temperature range of 120-180°C. More than one water molecule is responsible for the initial weight loss. While the second weight loss occurs in the 350–550°C and 180–350°C temperature ranges and is caused by the high temperature-induced collapse of the structure, the condensation of structural hydroxyl (-OH) groups, and the breakdown of organic moieties that result in the conversion of the dehydrated compound into metal pyrophosphate [19].

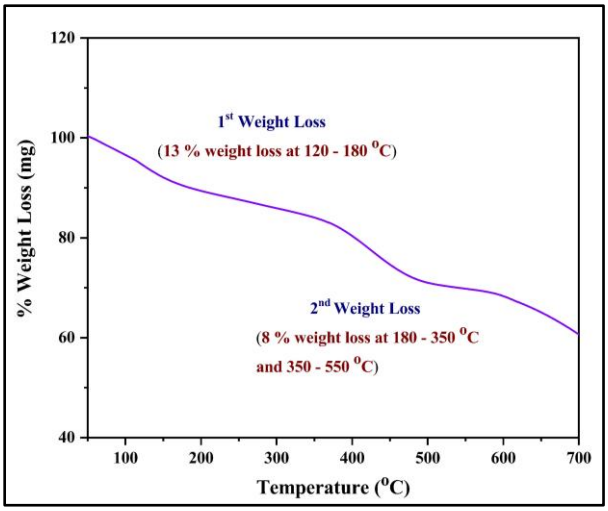

Figure 5.6. TGA Curve of Ce-ATMP.

5.3.5. XRD

XRD pattern of Ce-ATMP **(Figure 5.7)** indicates an amorphous nature due to the absence of sharp peaks. The observed peak at ~28 2θ (Two Theta) scale in illustrates the huge amount of amorphous carbon material present.

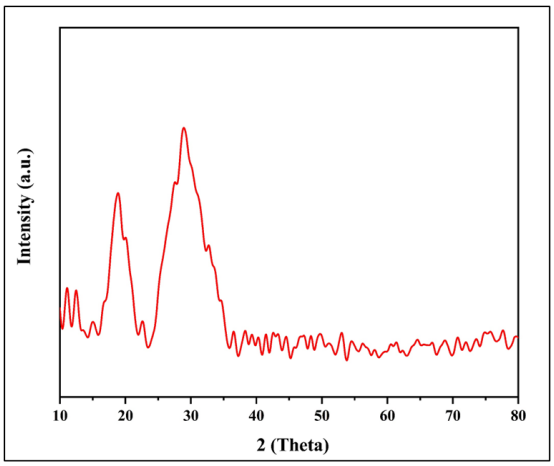

Figure 5.7. XRD Curve of Ce-ATMP.

5.3.6. FTIR Spectrum

The FTIR spectrum exhibits a broad spectrum at ~3300 cm^{-1}, owing to the -OH groups' symmetric and asymmetric O-H stretching vibrations, which are identified as defective P-OH groups since they represent exchangeable sites (H^+ of the -OH groups) [26]. Aquo H-O-H bending and aliphatic P=O stretching is responsible for the acute medium band at ~1633 cm^{-1} and the broad spectrum at ~1062 cm^{-1}, respectively. The existence of a secondary amine for ATMP, overlapped C-H bending of -CH_2 groups, and P-C stretching vibrations are the causes of the band in the range of ~1410 cm^{-1}. The metal oxide (Ce=O) bond is responsible for the peak at ~586 cm^{-1}, Ce-ATMP, Transition and heavy metal ions with loaded of Ce-ATMP were also seeing **(Figure 5.8 (a))**. The foregoing observations are further supported by the FT-IR spectra **(Figure 5.8 (b))** of the calcined samples, which might be interpreted as the elimination or reduction in intensity of the peaks at around ~3400 and ~1640 cm^{-1}, which are responsible for the -OH group [30].

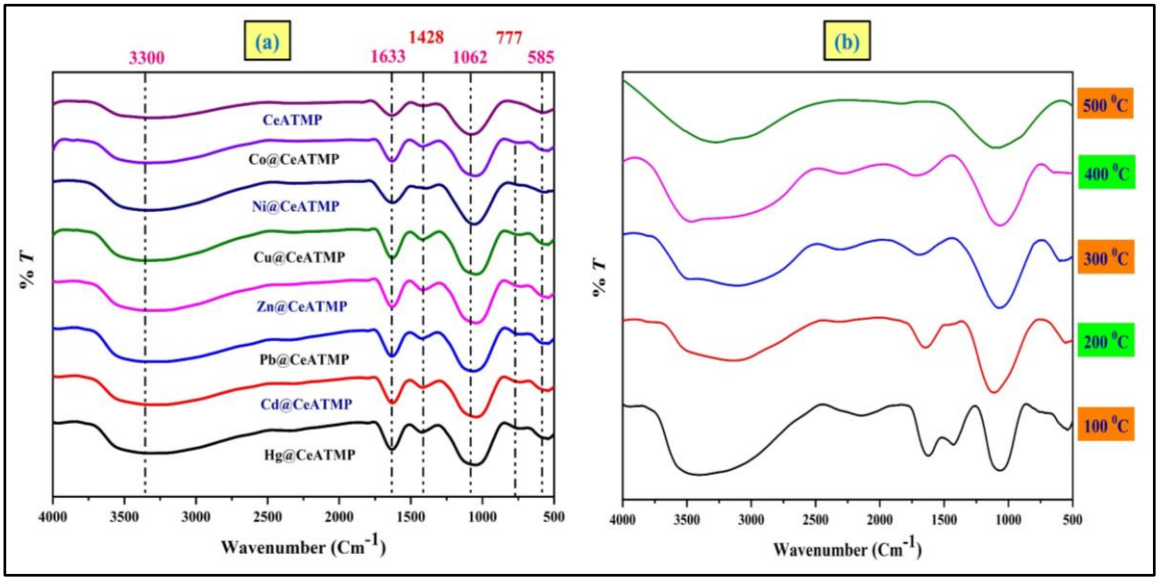

Figure 5.8. (a) FTIR spectra of Ce-ATMP loaded with Transition metal ions (Cu^{2+}, Ni^{2+}, Zn^{2+}, Co^{2+}) and Heavy metal ions (Pb^{2+}, Cd^{2+}, Hg^{2+}) and (b) FTIR spectra of Calcined Samples of Ce-ATMP with Varying Temperature, 100 ^{0}C, 200 ^{0}C, 300 ^{0}C, 400 ^{0}C, and 500 ^{0}C.

5.3.7. Distribution coefficient (K_d)

Distribution coefficient (K_d) values are influenced by the concentration of metal ions. **Table 5.2** exhibits this relationship, showing that K_d value increases up to 0.002 M and subsequently declines as the background solution's metal ion concentration rises (> 0.002 to 0.007 M). The availability of more exchangeable sites may be the cause of the first K_d value

rises in the lower concentration range. High metal ion concentrations result in an absence of sufficient sites, which causes the estimated K_d value to decline **(Figure 5.9)**. The optimum concentration is presented in **Table 5.2**.

Table 5.2. Distribution Coefficient (K_d) Values ($mL \cdot g^{-1}$) Varying the Metal Ions Concentrations (M) for Ce-ATMP.

Metal ions	Ionic radii (Å)	Distribution coefficient (K_d) values ($mL \cdot g^{-1}$) at different concentrations						
		0.001 M	**0.002 M**	0.003 M	0.004 M	0.005 M	0.006 M	0.007 M
Cu^{2+}	0.74	1400	**2150**	1587	1316	1150	1100	1074
Ni^{2+}	0.72	1025	**1300**	1100	1030	993	956	924
Zn^{2+}	0.74	950	**1185**	1025	962	900	861	833
Co^{2+}	0.72	800	**955**	900	870	854	823	800
Pb^{2+}	1.44	1233	**1600**	1255	1150	1087	1057	1014
Cd^{2+}	0.97	900	**1066**	1011	914	872	834	807
Hg^{2+}	1.10	740	**844**	833	800	768	763	700

Note: (i) Maximum deviation in K_d values = ±2.
(ii) Bold values are indicating optimal metal ion concentration for respective metal ion.

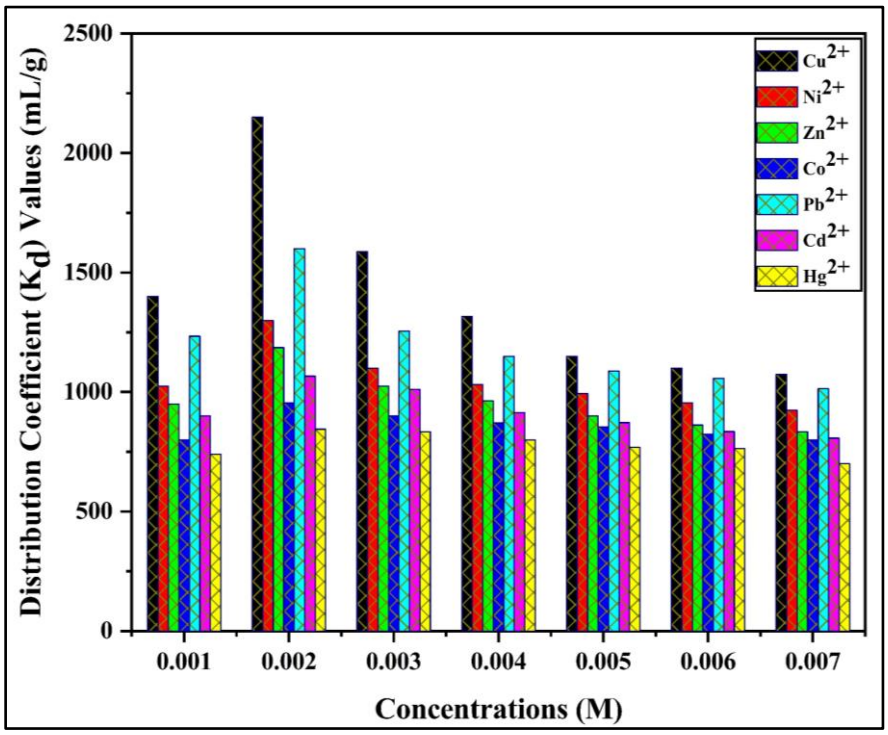

Figure 5.9. Distribution coefficient (K_d) values ($mL \cdot g^{-1}$) evaluated for transition and heavy metal ions (Cu^{2+}, Ni^{2+}, Zn^{2+}, Co^{2+}, Pb^{2+}, Cd^{2+}, Hg^{2+}) varying concentration in aqueous medium using Ce-ATMP.

Table 5.3 summarizes the K_d values obtained for the metal ions under investigation utilizing Ce-ATMP under ideal circumstances (maximum metal ion concentration, pH of maximum adsorption, and maximum equilibrium period) in the presence of an electrolyte. Higher electrolyte concentrations are generally associated with lower K_d levels, and vice versa. K_d values in strong electrolyte medium are lower than those in weak electrolyte and aqueous media. This might be explained by the intense ion competition in strong electrolyte mediums for exchange. K_d values in an aqueous media are arranged as follows: $Cu^{2+} > Ni^{2+} > Zn^{2+} > Co^{2+}$ for the transition metal ions and $Pb^{2+} > Cd^{2+} > Hg^{2+}$ for the heavy metal ions. High K_d values for Cu^{2+} and Pb^{2+} (aqueous medium) are among Ce-ATMP's most promising attributes. In contrast, K_d values for Co^{2+} and Hg^{2+} are extremely low in 0.2 M HNO_3,0.2 M $HClO_4$, and 0.2 M NH_4NO_3.

Table 5.3. BTC and K_d evaluated in aqueous and various electrolyte media using Ce-ATMP.

Metal Ions	BTC	Aq. media	K_d values (mL.g^{-1}) at different concentrations in different electrolytes							
			NH_4NO_3		HNO_3		$HClO_4$		CH_3COOH	
			0.02 M	0.2 M	0.02 M	0.2 M	0.02 M	0.2 M	0.02 M	0.2 M
Cu^{2+}	0.64	2150	1275	1150	757	450	940	733	1400	1100
Ni^{2+}	0.48	1300	1020	817	450	257	833	500	1200	940
Zn^{2+}	0.40	1186	1140	786	455	213	663	400	984	757
Co^{2+}	0.32	956	373	300	233	195	282	225	589	510
Pb^{2+}	0.56	1600	1200	1100	522	323	700	588	1100	900
Cd^{2+}	0.30	1067	933	757	306	200	675	370	829	633
Hg^{2+}	0.18	844	218	190	150	120	200	160	364	225

5.3.8. Breakthrough Capacity (BTC)

A breakthrough curves (plots of C_e/C_0 vs. effluent volume) for transition metal ions and heavy metal ions are presented in **Figure 5.10 (a and b)**. The dynamic or operating capacity of a known quantity of ion-exchange material towards metal ions in column operation is known as breakthrough capacity (BTC). The factors that primarily affect the exchange of a specific metal ion in a dynamic process include temperature, particle size, bed depth, selectivity coefficient, contact time, and feed solution flow rate through the column. The affinity of a metal ion toward the ion exchanger, which is established by a batch procedure, is also indicated by K_d values. **Table 5.3** illustrates the expected equality of the metal-ion affinities towards the exchanger based on K_d and BTC.

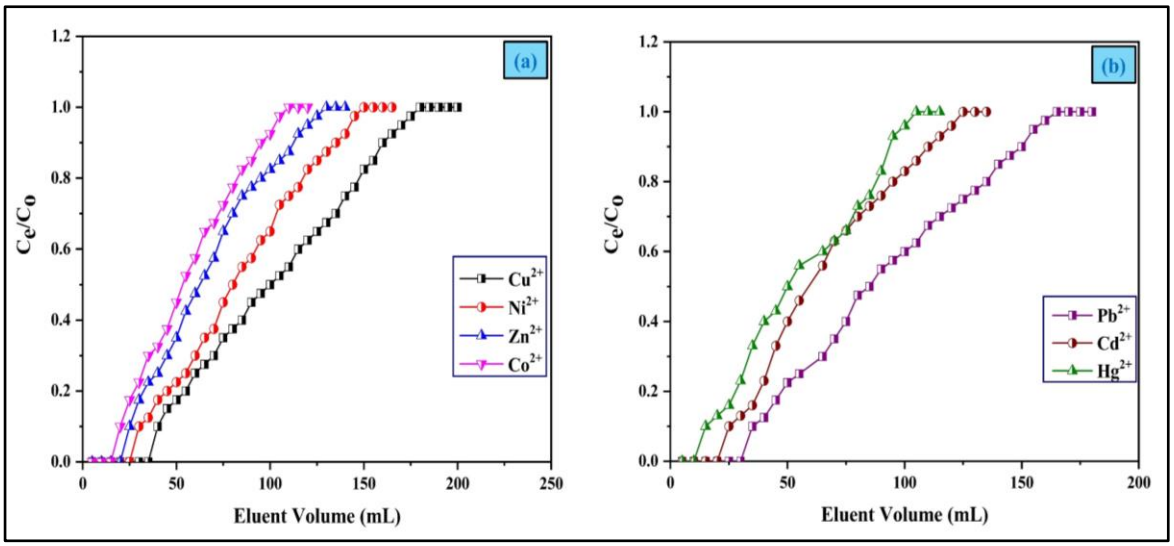

Figure 5.10. (a) BTC of transition metal ions (Cu^{2+}, Ni^{2+}, Zn^{2+}, Co^{2+}) (b) BTC of Heavy metal ions (Pb^{2+}, Cd^{2+}, Hg^{2+}) using Ce-ATMP.

5.3.9. Adsorption studies

5.3.9.1. Contact time and effects of pH

For the intent of optimizing the ion exchange of the metal ions under study utilizing the ion exchanger Ce-ATMP, the effects of experimental variables including contact time and pH were investigated. K_d value rises throughout contact time (up to 60 min) and then fully sorbs on Ce-ATMP for 24 hours, at which point K_d value does not rise any further **(Table 5.4)**. Very little sorption for all metal ions has been detected at pH levels below about 3 **(Table 5.5, Figure 5.11)**. Due to the fact that there is more hydrogen ions than metal ions striving for sorption/exchange sites, sorption is inhibited at lesser pH levels.

Table 5.4. Effect of contact time on the K_d value of metal ions using Ce-ATMP.

Metal Ions	Equilibrium values (mequie·g^{-1})							
	10 min	20 min	30 min	40 min	50 min	60 min	70 min	80 min
Cu^{2+}	0.94	0.95	0.96	0.98	0.99	1	1	1
Ni^{2+}	0.94	0.95	0.96	0.97	0.99	1	1	1
Zn^{2+}	0.94	0.95	0.96	0.98	0.99	1	1	1
Co^{2+}	0.93	0.95	0.97	0.98	0.98	1	1	1
Pb^{2+}	0.94	0.95	0.96	0.96	0.99	1	1	1
Cd^{2+}	0.92	0.94	0.95	0.97	0.98	1	1	1
Hg^{2+}	0.93	0.95	0.96	0.98	0.99	1	1	1

Table 5.5. Percentage uptake of metal ions with varying pH using Ce-ATMP.

pH	Uptake of metal ion (%)						
	Cu^{2+}	Ni^{2+}	Zn^{2+}	Co^{2+}	Pb^{2+}	Cd^{2+}	Hg^{2+}
1	27.78	17.86	14.44	11.58	20.00	12.86	10.59
2	44.44	34.52	32.22	28.42	41.18	30.00	23.53
3	**72.22**	**65.48**	46.67	42.11	**69.41**	44.29	**35.29**
4	66.67	60.71	**55.56**	**46.32**	64.71	**50.00**	27.06
5	61.11	54.76	43.33	29.47	58.82	31.43	23.53
6	54.44	50.00	35.56	26.32	52.94	28.57	21.18
7	-	-	-	-	-	-	-

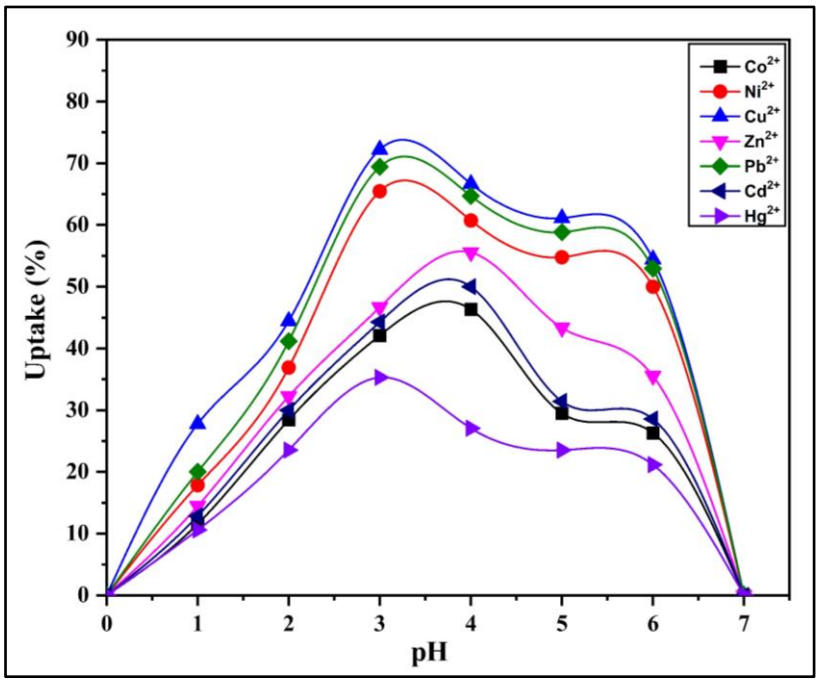

Figure 5.11. pH values of Ce-ATMP with transition and heavy metal ions.

5.3.9.2. Adsorption isotherm

The relationship between the quantities of the metal ions adsorbed and the concentration equilibrium (C_e) can be obtained using the linear form of the Langmuir isotherm (most commonly used adsorption isotherm models) as previously stated in “Chapter 3" (Sec. 3.3.5).

The isotherm constants are essential for comprehending the adsorption process and for using them to anticipate a few essential design parameters. The Langmuir isotherms are

plotted against $C_e/(X/V_m)$ *versus* C_e to create straight lines from which the constants can be extracted based on the intercepts and slopes. **Table 5.6** presents the Langmuir constants (b and V_m) derived from the linear plots' slopes and intercepts.

Table 5.6. Langmuir constants evaluated for transition and heavy metal ions using Ce-ATMP

Metal Ions	Temperature (°C)	Langmuir constants			
		R^2	b ($dm^3.mg^{-1}$)	V_m ($mg.g^{-1}$)	R_L
Co^{2+}	27	0.946	0.0023	15.72	0.971
	37	0.981	0.0034	16.10	0.963
	47	0.975	0.0037	17.42	0.954
	57	0.983	0.0038	19.69	0.953
Ni^{2+}	27	0.994	0.0025	17.51	0.989
	37	0.998	0.0034	17.73	0.978
	47	0.996	0.0036	20.00	0.972
	57	0.999	0.0042	20.40	0.963
Cu^{2+}	27	0.998	0.0030	26.04	0.963
	37	0.999	0.0039	26.53	0.952
	47	0.999	0.0044	28.99	0.951
	57	0.996	00058	29.24	0.940
Zn^{2+}	27	0.994	0.0024	16.84	0.975
	37	0.988	0.0026	17.92	0.967
	47	0.982	0.0031	18.73	0.963
	57	0.979	0.0038	18.87	0.953
Cd^{2+}	27	0.999	0.0035	33.78	0.970
	37	0.998	0.0038	36.36	0.962
	47	0.997	0.0043	39.06	0.960
	57	0.998	0.0059	42.01	0.951
Hg^{2+}	27	0.989	0.0022	32.46	0.977
	37	0.990	0.0030	33.00	0.969
	47	0.993	0.0036	34.96	0.963
	57	0.993	0.0049	36.23	0.950
Pb^{2+}	27	0.999	0.0059	69.93	0.945
	37	0.998	0.0067	74.07	0.934
	47	0.998	0.0096	76.92	0.904
	57	0.999	0.0169	78.13	0.895

Regarding the sorption of transition and heavy metal ions under investigation in this work, Langmuir isotherms are deemed suitable when the R^2 value hovers near unity. The values of R^2 demonstrate that the Langmuir isotherms offer good fits to the experimental data. An advantageous adsorption is given by low values of b in the current study. According to the order of transition metal ions ($Cu^{2+} > Ni^{2+} > Zn^{2+} > Co^{2+}$) and heavy metal ions ($Pb^{2+}$

> Cd^{2+} > Hg^{2+}) at 303-333 K, the exchanger's maximum adsorption capacities, or V_m values, correspond to the following: normal isotherms and advantageous adsorption (between 0 and 1). These outcomes align with earlier findings [31]. As illustrated in **(Figures 5.12 and 5.13)**, transition metal Cu^{2+} and heavy metal Pb^{2+} are displayed. The metal figures for Ni^{2+}, Zn^{2+}, Co^{2+}, Cd^{2+}, and Hg^{2+} are shown in **(Figures 5.14 and 5.15)**.

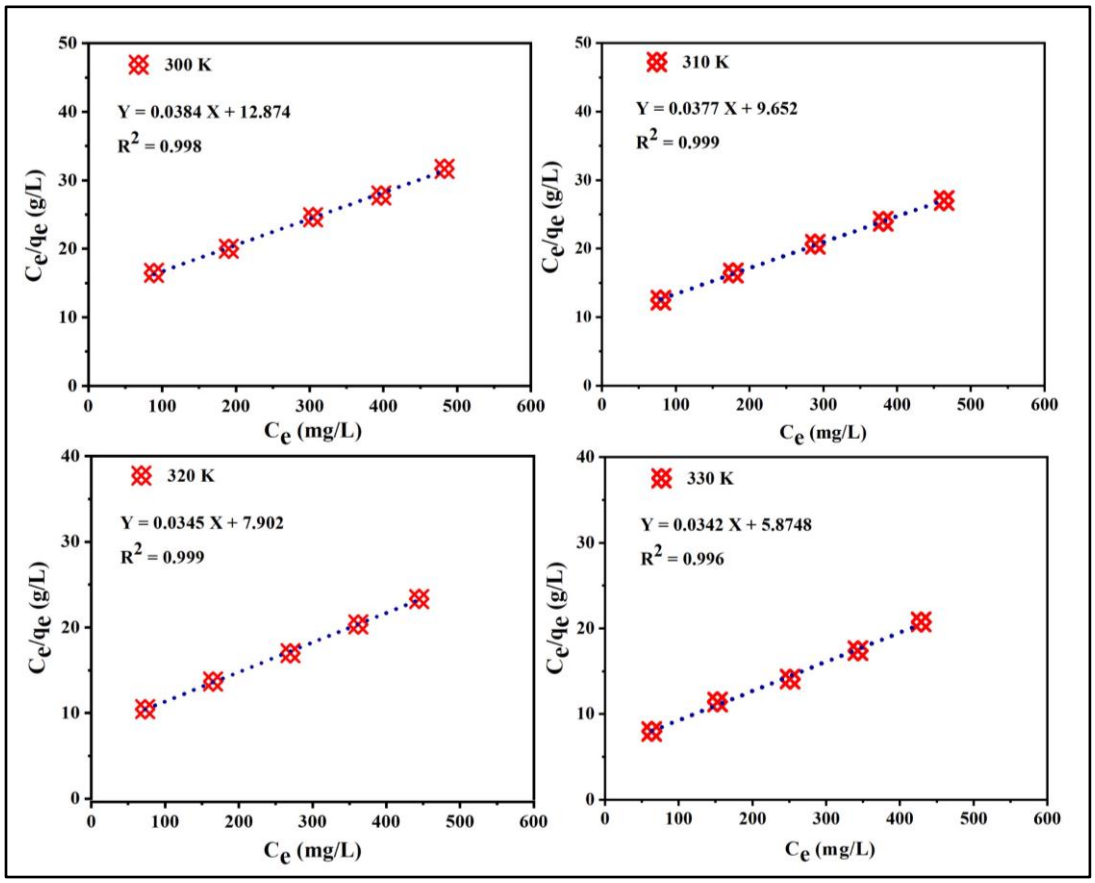

Figure 5.12. Langmuir adsorption isotherms of transition metal ion (Cu^{2+}) 300, 310, 320 and 330 K.

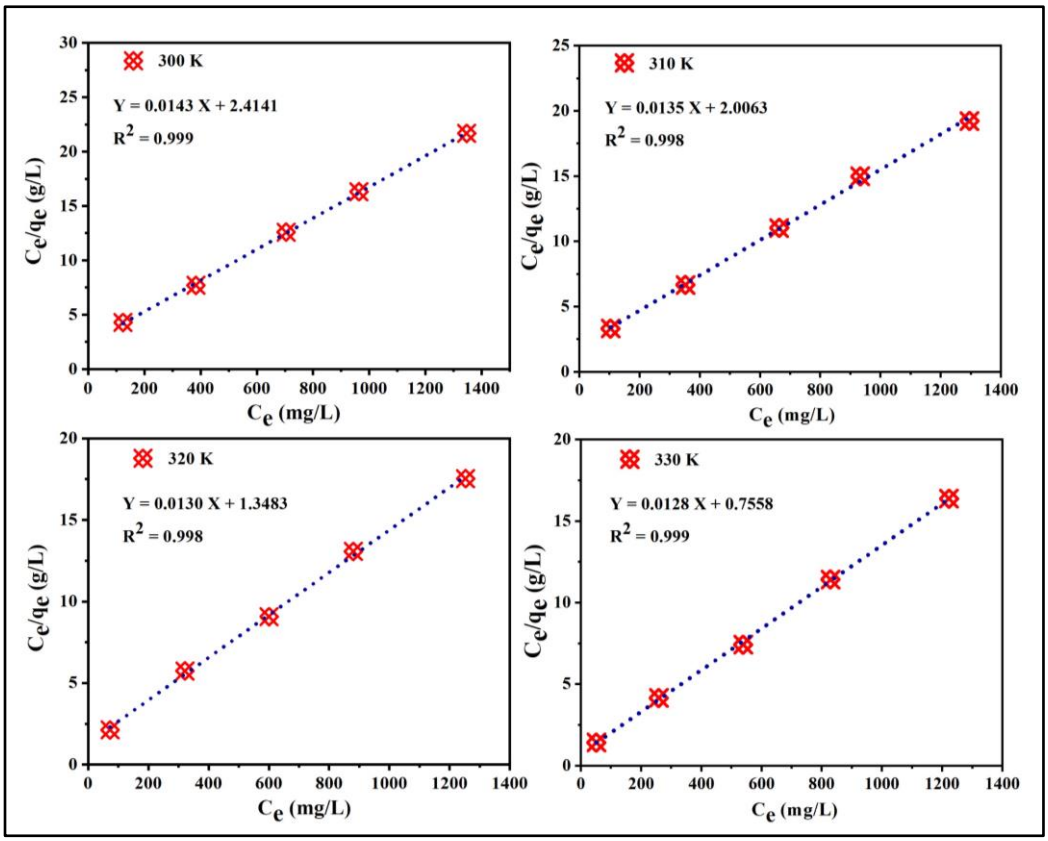

Figure 5.13. Langmuir adsorption isotherms of heavy metal ion (Pb^{2+}) 300, 310, 320 and 330 K.

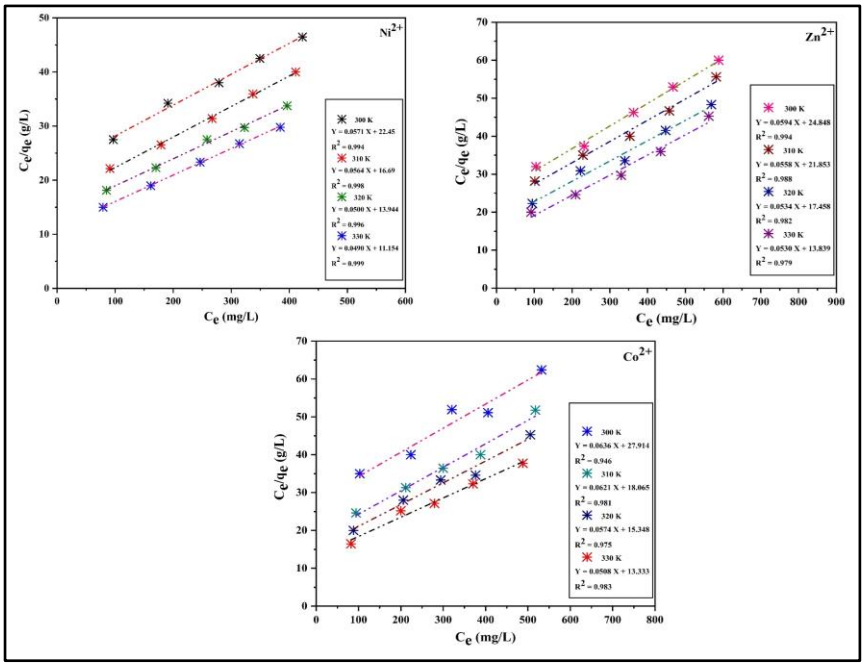

Figure 5.14. Langmuir adsorption isotherms of Transition metal ions (Ni^{2+}, Zn^{2+} and Co^{2+}) 300, 310, 320 and 330 K.

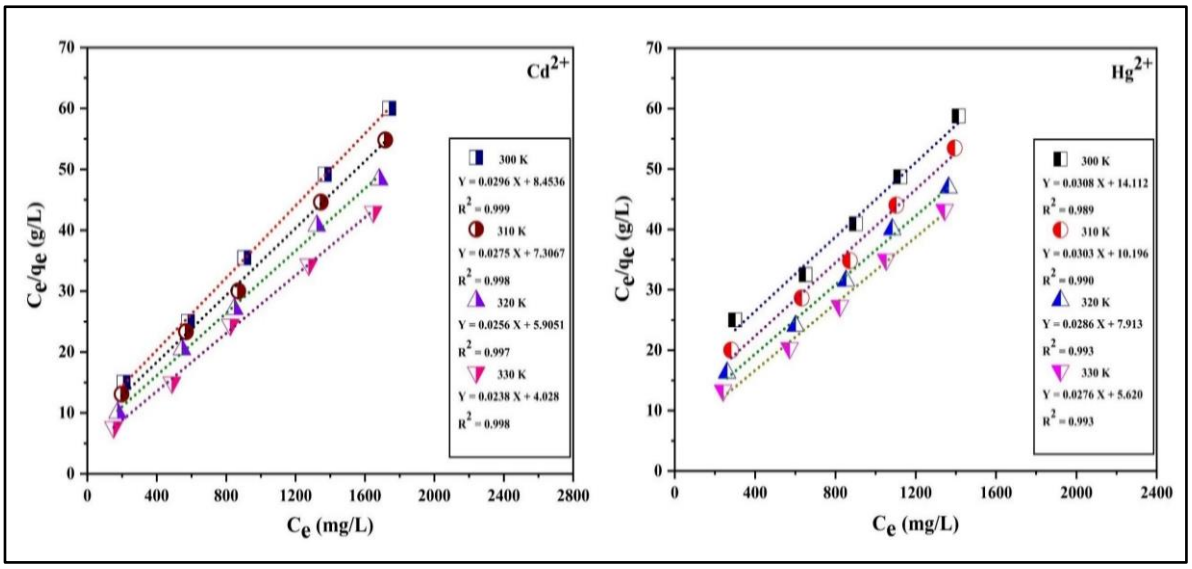

Figure 5.15. Langmuir adsorption isotherms of Heavy metal ions (Cd^{2+} and Hg^{2+}) 300, 310, 320 and 330 K.

5.3.9.3. Thermodynamics of ion exchange using Ce-ATMP

Thermodynamics of Ce-ATMP has been investigated for transition metal ions Cu^{2+}, Zn^{2+}, Co^{2+}, Ni^{2+} as well as heavy metal ions Pb^{2+}, Cd^{2+}, Hg^{2+}. Standard formulas have been employed for assessing parameters like the K, ΔG°, ΔH°, and ΔS°. The findings are shown in **Table 5.7**.

All of the equilibrium investigations were conducted after the samples were kept shaken for 60 minutes, as indicated by a plot of the fractional attainment of equilibrium U(τ) vs time (t) **(Figure 5.16)**. This indicates that the exchange equilibrium for Ce-ATMP was presumably reached in within that time.

The current investigation revealed that the equilibrium constant (K) increased as the temperature rise for every metal ion evaluated **(Table 5.7)**, suggesting that ion exchange is the mechanism at work and that the metal ions had a strong affinity for the exchanger. The exchanger exhibits a higher preference for metal ions than H^+ ions, as evidenced by the fact that ΔG° for all metal exchange processes was found to be negative throughout the temperature range. It was confirmed that the exchange was more favorable as the temperature rise by looking at the ΔG° readings, which become more negative. The method was endothermic since ΔH° was positive in every instance. A higher enthalpy change indicates that the exchange process is more endothermic and that more energy is needed for dehydration to take place. The cation needs energy when it exits the hydration sphere to undertake ion exchange because ion exchange requires dehydration [32]. In the case of Cu^{2+} among

transition metal ions and Pb^{2+} among heavy metal ions, the ΔH° values imply that total dehydration certainly takes place. The significant negative ΔG° values for Cu^{2+} and Pb^{2+} are consistent with these observations. Along with ΔH°, ΔS° for all metal ions likewise exhibits the same tendency. Wider dehydration, indicating greater disorder caused during the exchange, is the reason for the larger ΔS° values also seen in the case of Cu^{2+} and Pb^{2+}.

Table 5.7. Thermodynamic Parameters Assessed Evaluated for M^{2+}-H^{+} Exchange at Various Temperatures Using Ce-ATMP.

Metal Ions	Temperature (°C)	K	ΔG° (kJ.mol^{-1})	ΔH° (kJ.mol^{-1})	ΔS° (J.mol^{-1}.°C^{-1})
Co^{2+}-H^{+}	27	2.35	-1.06	7.22	27.72
	37	2.37	-1.11		26.97
	47	2.40	-1.16		26.28
	57	2.42	-1.21		25.63
Ni^{2+}-H^{+}	27	1.82	-0.74	36.14	123.39
	37	1.88	-0.81		119.61
	47	1.95	-0.89		116.11
	57	2.07	-1.00		112.91
Cu^{2+}-H^{+}	27	2.01	-0.87	66.25	224.52
	37	2.21	-1.01		217.73
	47	2.33	-1.12		211.22
	57	2.58	-1.30		205.34
Zn^{2+}-H^{+}	27	2.13	-0.94	23.77	82.65
	37	2.24	-1.04		80.29
	47	2.25	-1.07		77.89
	57	2.33	-1.16		75.78
Cd^{2+}-H^{+}	27	1.99	-0.85	28.88	99.45
	37	2.05	-0.92		96.46
	47	2.14	-1.01		93.70
	57	2.21	-1.08		91.08
Hg^{2+}-H^{+}	27	2.32	-1.04	19.03	67.18
	37	2.38	-1.11		65.22
	47	2.43	-1.18		63.39
	57	2.49	-1.25		61.67
Pb^{2+}-H^{+}	27	2.12	-0.93	48.47	165.27
	37	2.22	-1.02		160.22
	47	2.35	-1.13		155.53
	57	2.54	-1.27		151.24

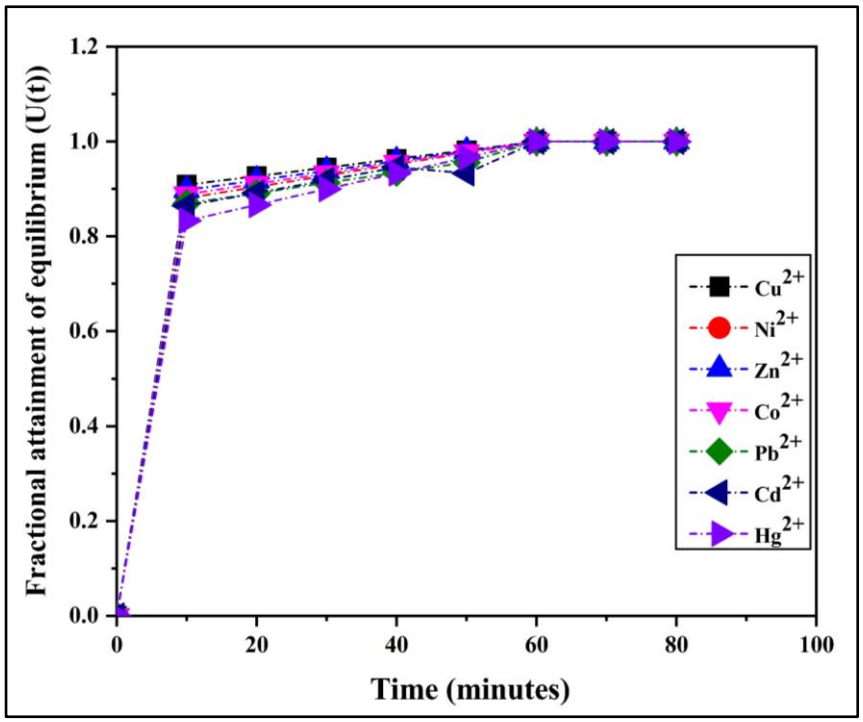

Figure 5.16. Fractional attainment of equilibrium for varying metal ions *versus* time using Ce-ATMP.

5.3.9.4. Kinetics study using Ce-ATMP

The pseudo-first-order, pseudo-second-order, and intra-particle diffusion models were utilized in order to explore the transition and heavy metal ion's adsorption process on Ce-ATMP. In **Table 5.8**, kinetic parameters are displayed. The standard adsorption kinetics for Cu^{2+} ions are displayed in **Figure 5.17**. It is evident that metal ion adsorption onto Ce-ATMP occurred quickly in the first 15 min and progressively approached equilibrium in the following 60 min. Data analysis reveals remote R^2 values from 1, indicating that pseudo-first-order is not relevant. However, matching of the predicted and experimental q_e values, as well as a strong correlation coefficient (Cu^{2+} = 0.9995), appear in the pseudo-second-order equation results **(Table 5.8)**. As a result, it is probable that the ion exchange process can be explained by pseudo-second-order kinetics. The intra-particle diffusion Weber-Morris model was also used to assess the kinetic data. Intraparticle diffusion contributes to a linear plot of q_t vs. the square root of time ($t^{0.5}$). Moreover, the origin should be crossed by such linear plots. The intraparticle diffusion model appears to be invalid for interpreting the current adsorption kinetics, as indicated by the R^2 value (Cu^{2+} = 0.9865) and the lack of a straight line extending from the origin. According to the explanation above, a pseudo-second-order chemical pathway influences the adsorption of transition and heavy metal ions. The graphs of each

kinetic model are displayed in **(Figures 5.18-5.20)** [32-34].

Table 5.8. Kinetic parameters of metal ion sorption onto Ce-ATMP.

Models	Parameters	Co^{2+}	Ni^{2+}	Cu^{2+}	Zn^{2+}	Cd^{2+}	Hg^{2+}	Pb^{2+}
Pseudo first order	K_1	0.0197	0.0192	0.0194	0.0185	0.0193	0.0184	0.0191
	q_e (cal)	0.0995	0.0942	0.0963	0.0888	0.0958	0.0882	0.0937
	R^2	0.9249	0.9178	0.9217	0.9023	0.9119	0.9001	0.9167
Pseudo second order	K_2	0.8748	0.6189	0.5228	0.7683	0.2614	0.5713	0.6870
	q_e (cal)	0.8613	0.7808	0.7509	0.8063	0.6416	0.7604	0.8007
	R^2	0.9996	0.9995	0.9995	0.9996	0.9992	0.9995	0.9995
Interparticle diffusion	K_{id}	0.0117	0.0113	0.0116	0.0103	0.0121	0.0102	0.0112
	C	0.7670	0.6902	0.6578	0.7463	0.5444	0.6769	0.7108
	R^2	0.9856	0.9904	0.9865	0.9796	0.9793	0.9765	0.9908
Experimental	q_e (exp)	0.8600	0.7800	0.7500	0.8300	0.6400	0.7600	0.8000

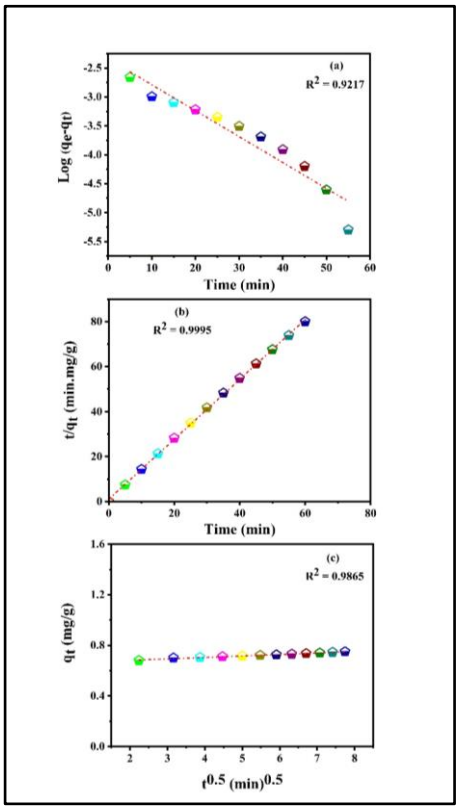

Figure 5.17. (a) Pseudo-first-order kinetics, (b) Pseudo-second-order kinetics and (c) Intraparticle diffusion model for adsorption of transition metal ion (Cu^{2+}) on Ce-ATMP.

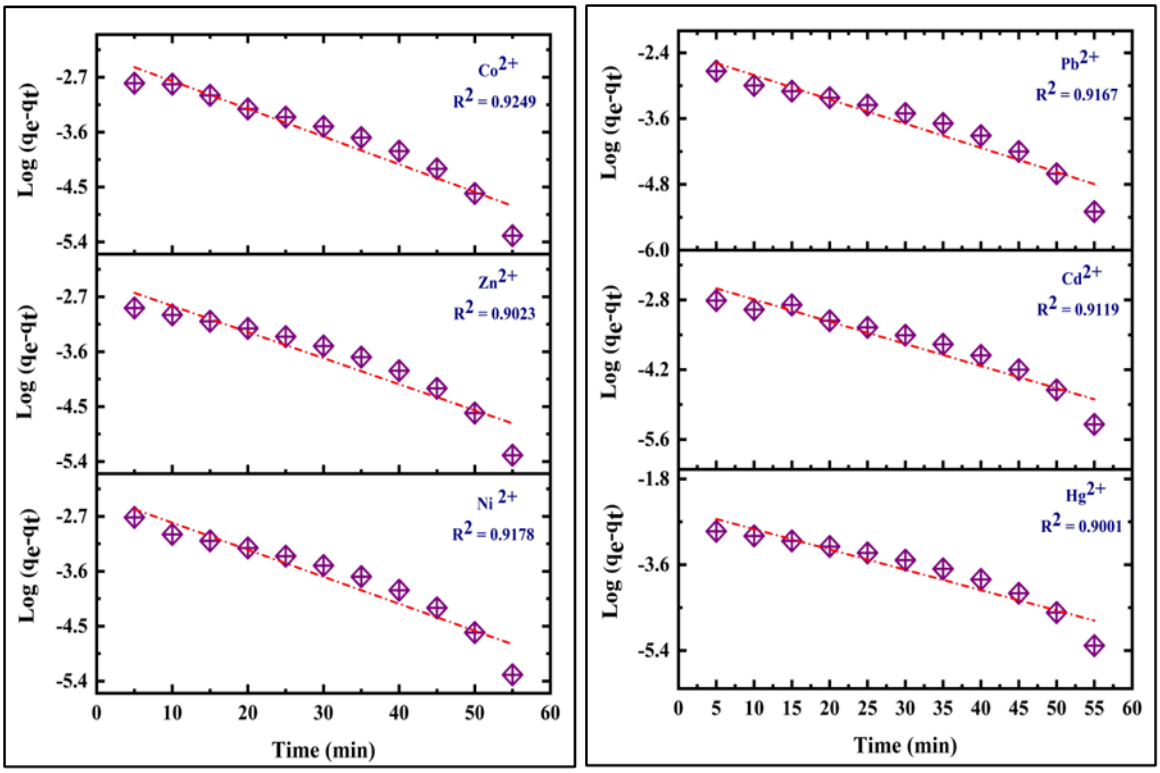

Figure 5.18. Pseudo-first-order kinetics for adsorption of transition metal ions (Ni^{2+}, Zn^{2+} and Co^{2+}) and Heavy metal ions (Pb^{2+}, Cd^{2+} and Hg^{2+}) on Ce-ATMP.

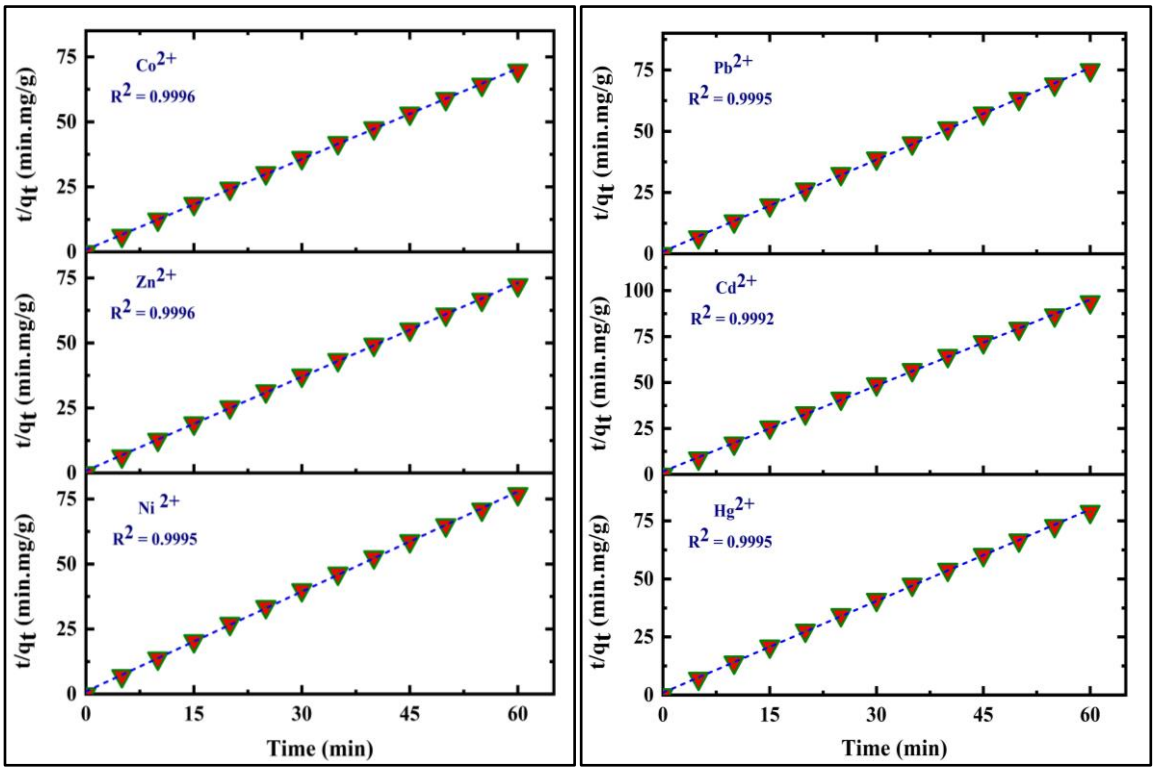

Figure 5.19. Pseudo-second-order kinetics for adsorption of transition metal ions (Ni^{2+}, Zn^{2+} and Co^{2+}) and Heavy metal ions (Pb^{2+}, Cd^{2+} and Hg^{2+}) on Ce-ATMP.

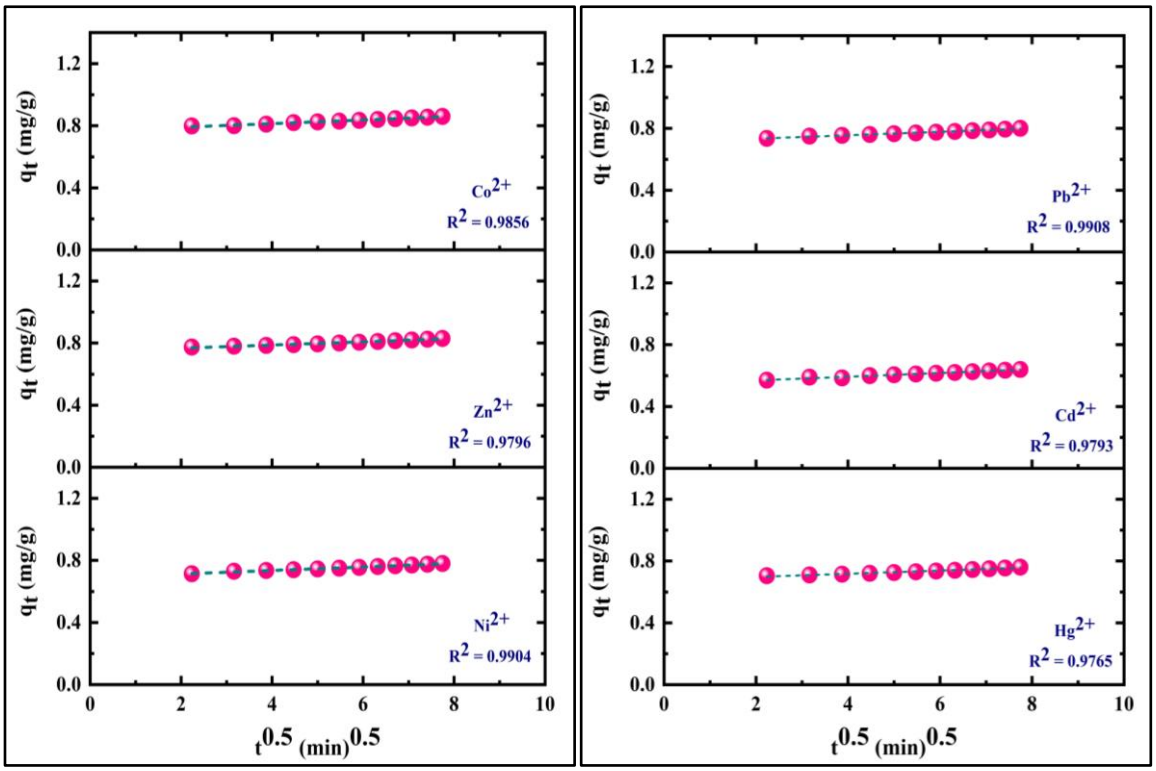

Figure 5.20. Intraparticle diffusion model for adsorption of transition metal ions (Ni^{2+}, Zn^{2+} and Co^{2+}) and Heavy metal ions (Pb^{2+}, Cd^{2+} and Hg^{2+}) on Ce-ATMP.

5.3.9.5. Elution of Ce-ATMP

Table 5.9 summarizes the behavior of transition and heavy metal ions during single elution, utilizing variable electrolyte media including ammonium nitrate, perchloric acid, glacial acetic acid, and nitric acid and different concentrations. In every instance, the percentage of metal eluted lies within 75-98%. The solitary metal ion present and the absence of other elements' interference allowed for good elution to be seen. Improved eluents have higher acid and eluent concentrations. It was discovered that 0.2 M HNO_3 was the most effective eluant for the majority of metal ions. Using 0.2 M HNO_3, the transition metal ions percentages of metal eluted were $Co^{2+} > Zn^{2+} > Ni^{2+} > Cu^{2+}$ while the heavy metal ions' percentages were $Hg^{2+} > Cd^{2+} > Pb^{2+}$. These findings complement the idea that metal ions with high K_d values are less eluted and vice versa [35]. Elution efficiency was demonstrated by the symmetrical bell shapes seen in the transition and heavy metal of the all metal ions elution curve **(Figure 5.21- 5.27)**.

Table 5.9. Percentage Elution (% E) of metal ions in different electrolyte media using Ce-ATMP.

Metal Ions	Percentage elution (% E) of metal ions in different electrolyte media							
	NH_4NO_3		HNO_3		$HClO_4$		CH_3COOH	
	0.02 M	0.2 M	0.02 M	0.2 M	0.02 M	0.2 M	0.02 M	0.2 M
Cu^{2+}	78.8	83.3	87.7	90.0	80.0	85.5	74.4	82.2
Ni^{2+}	78.5	80.9	90.4	91.6	85.7	89.2	75.0	85.7
Zn^{2+}	84.4	90.0	92.2	94.4	94.4	93.3	85.5	92.2
Co^{2+}	92.6	95.7	94.7	96.8	92.6	93.6	88.4	91.5
Pb^{2+}	82.3	88.2	90.5	91.7	88.2	89.4	77.6	85.8
Cd^{2+}	85.7	91.4	90.0	93.6	88.5	92.8	78.5	87.1
Hg^{2+}	88.2	91.7	92.9	97.6	89.4	92.9	87.0	90.5

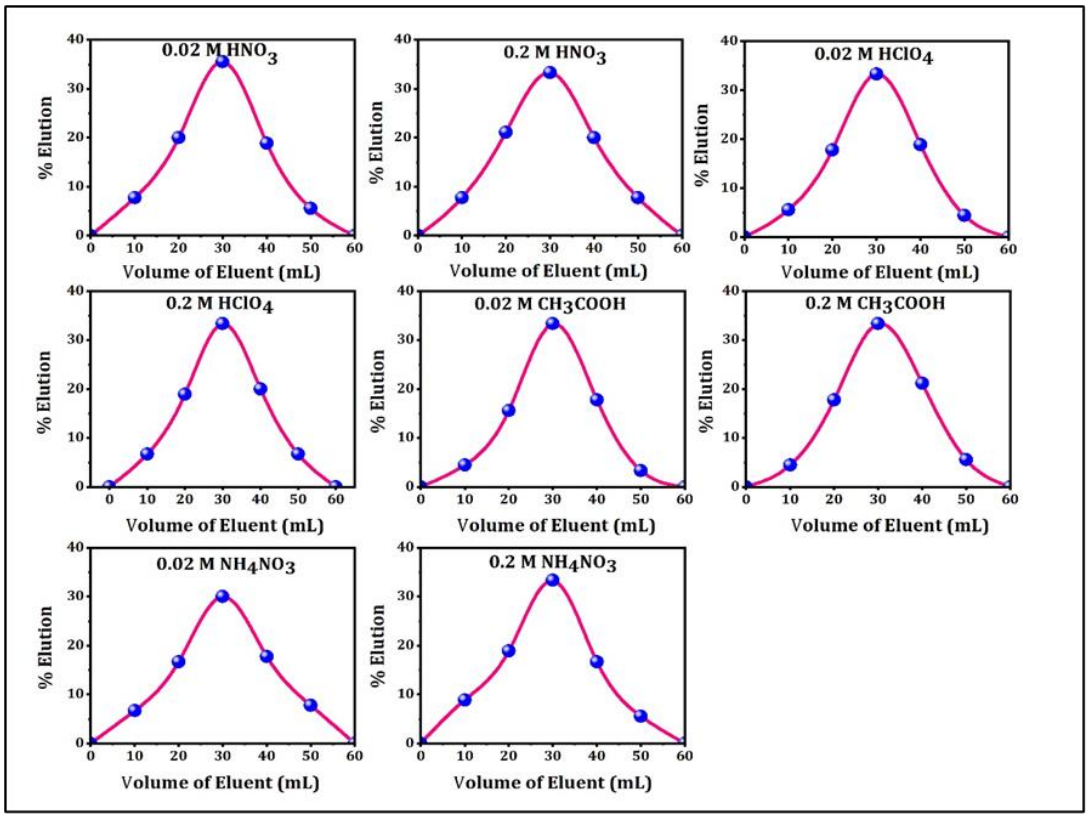

Figure 5.21. Elution curve of Cu^{2+} using Ce-ATMP.

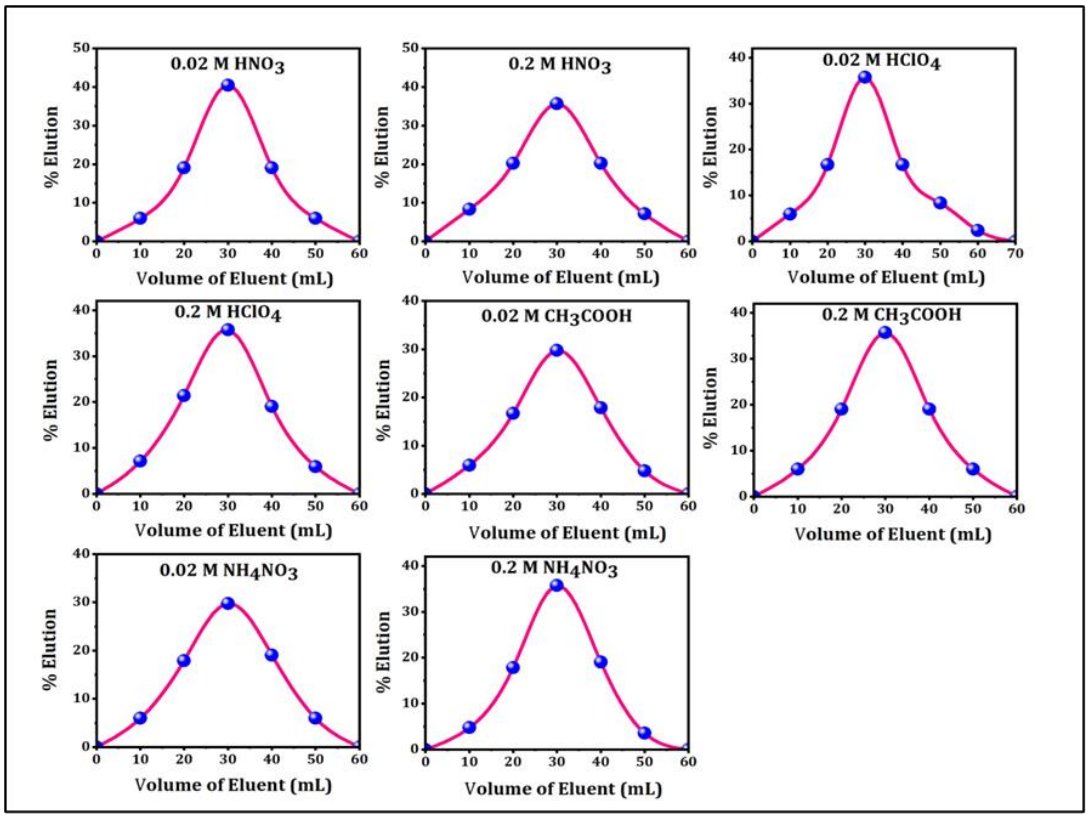

Figure 5.22. Elution curve of Ni^{2+} using Ce-ATMP.

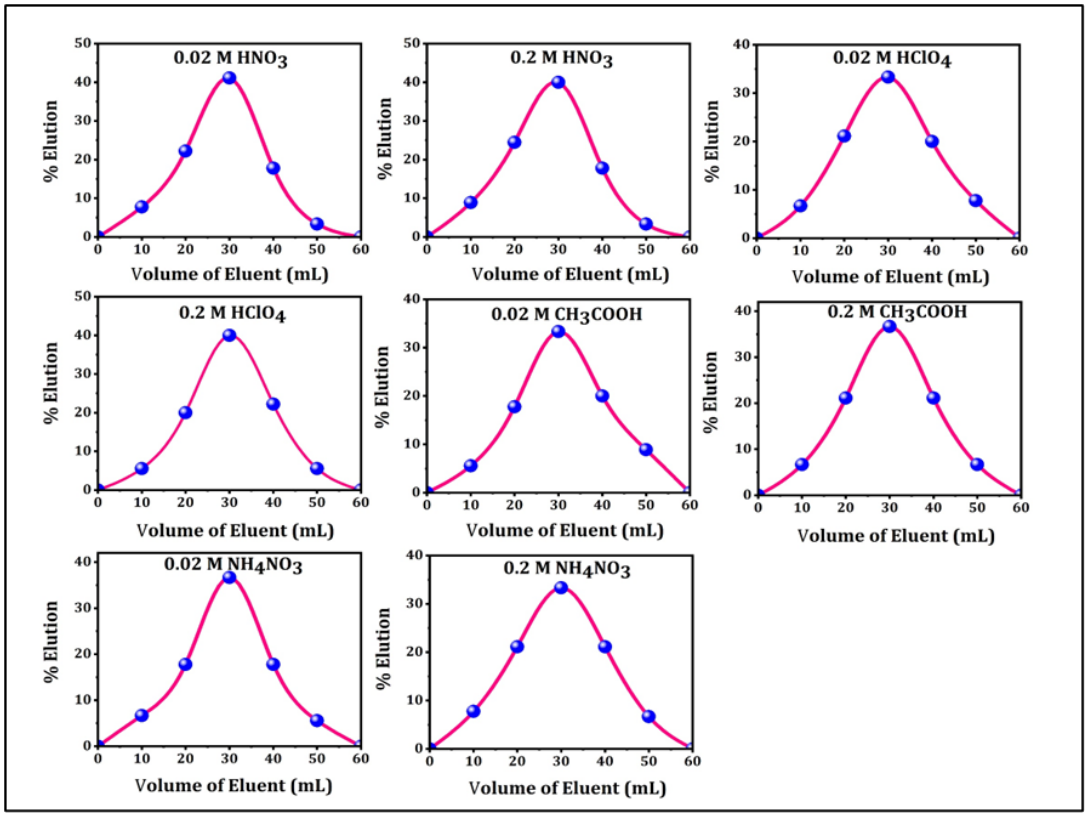

Figure 5.23. Elution curve of Zn^{2+} using Ce-ATMP.

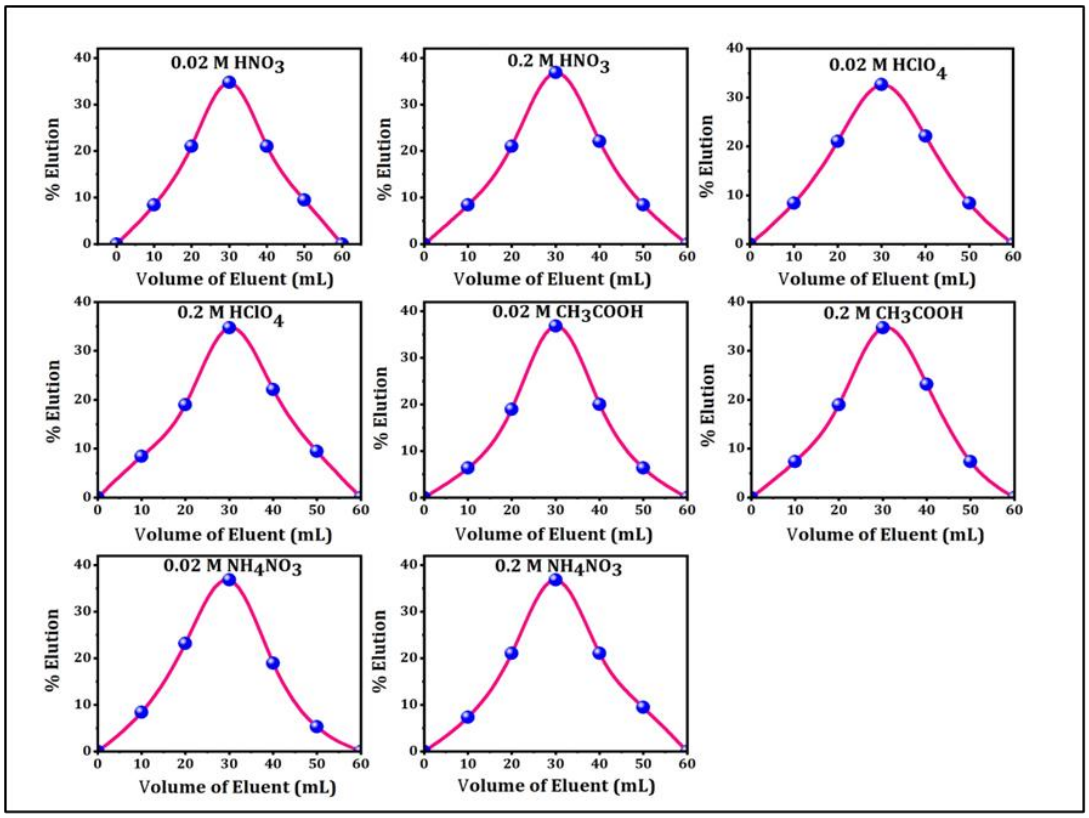

Figure 5.24. Elution curve of Co^{2+} using Ce-ATMP.

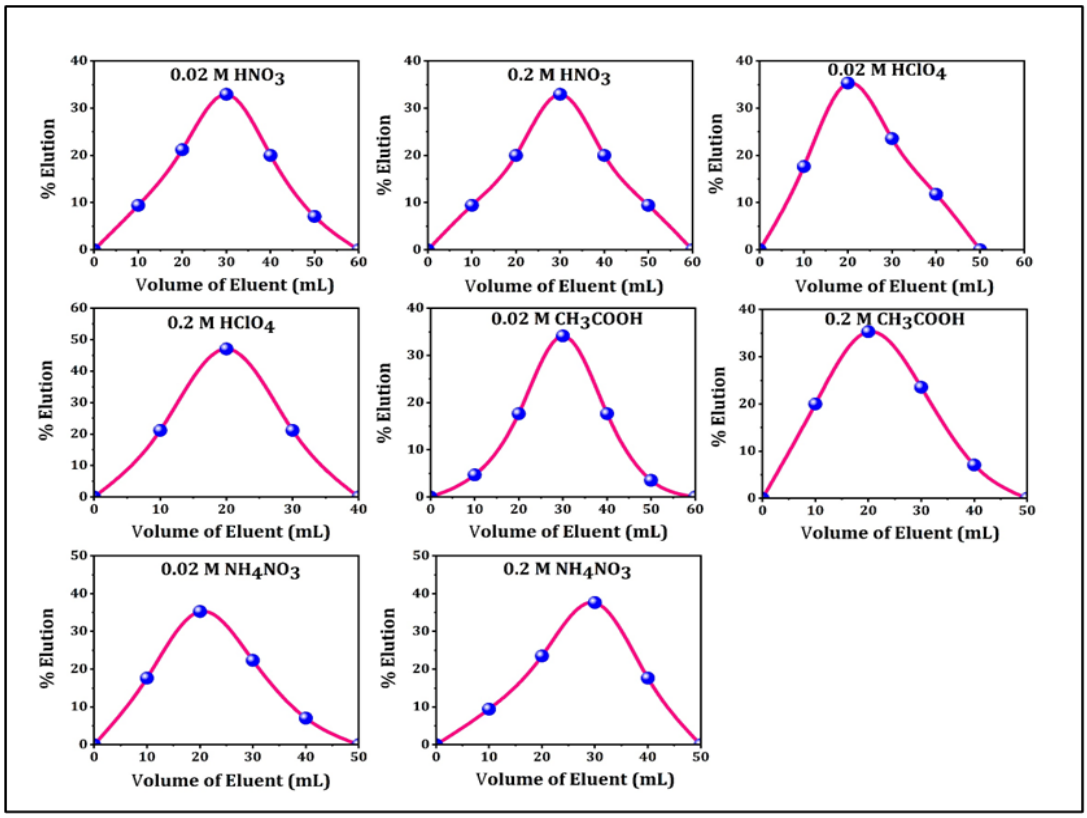

Figure 5.25. Elution curve of Pb^{2+} using Ce-ATMP.

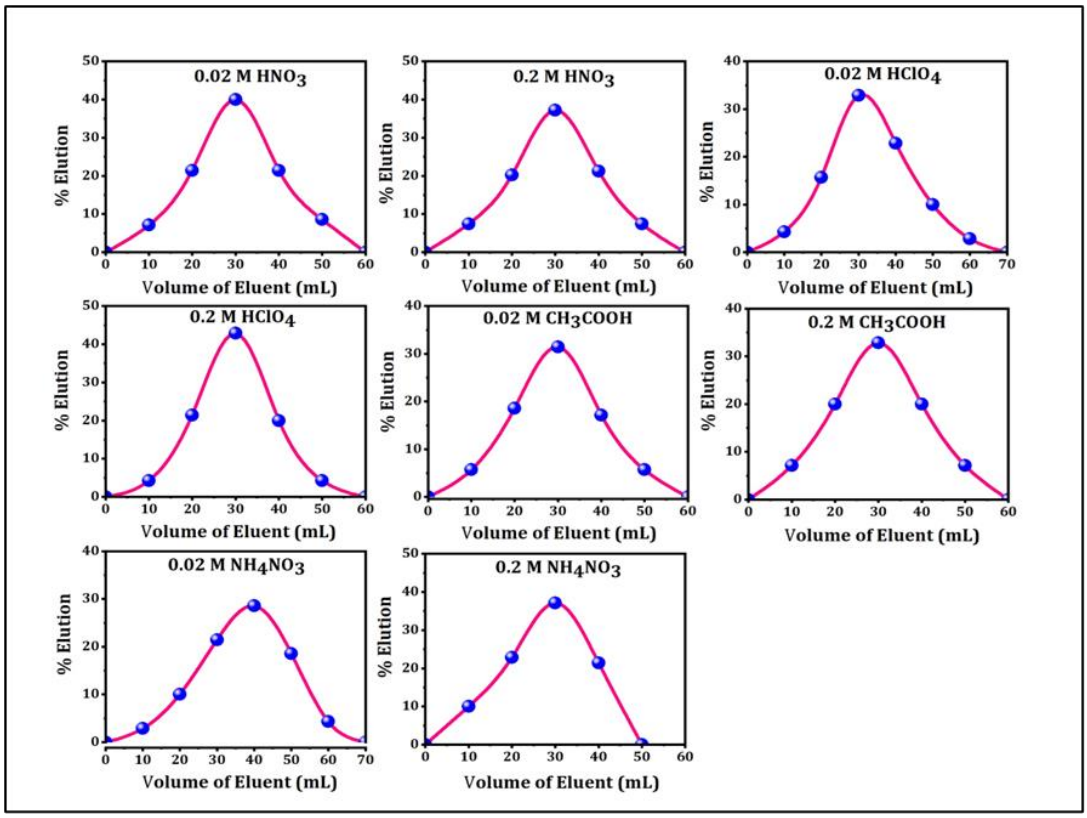

Figure 5.26. Elution curve of Cd^{2+} using Ce-ATMP.

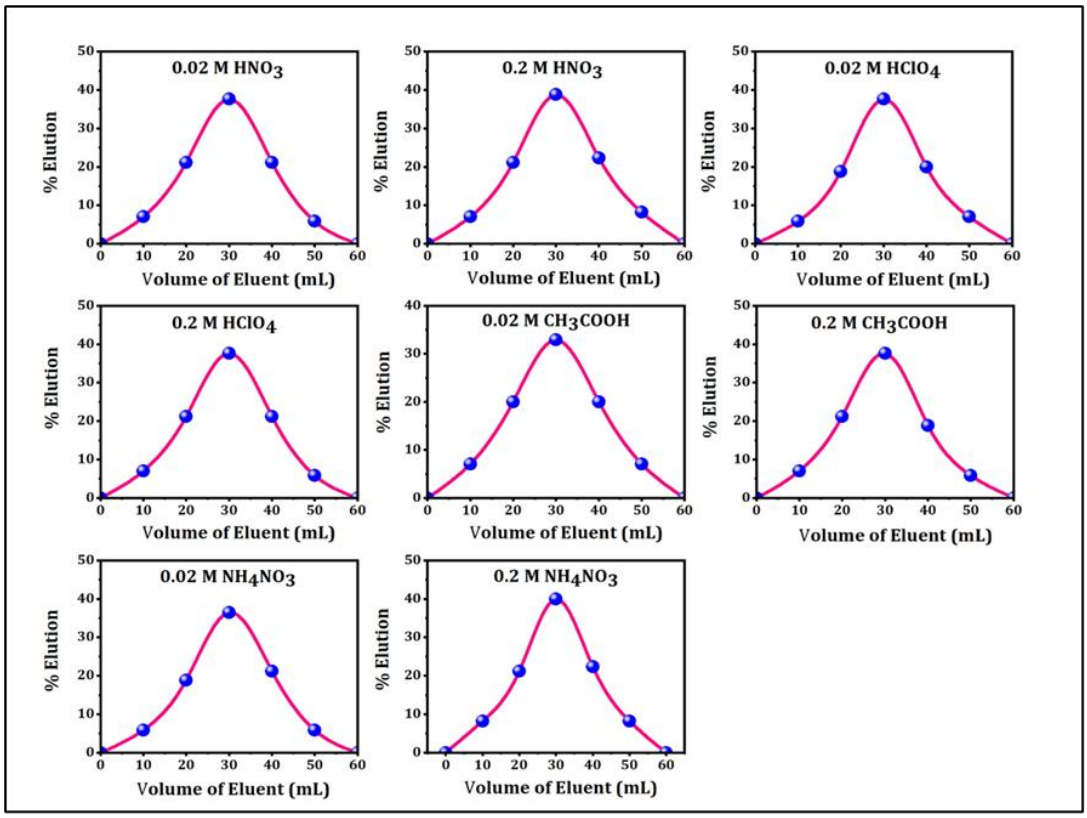

Figure 5.27. Elution curve of Hg^{2+} using Ce-ATMP.

5.3.9.6. Separations of Ce-ATMP

Metal separation is governed by the separation factor α, or the rate at which two constituents separate on a column, which is provided by the Equation 3:

$$\alpha = \frac{K_{d1}}{K_{d2}} \quad (3)$$

where K_{d1} and K_{d2} are the distribution coefficients of the two constituents being separated. Better separation is indicated by a larger α departure from unity. The conditions under which α has a beneficial value or influences the system in a way that is favorable to separation determine the effectiveness of an ion-exchange separation. The electrolyte medium with the highest separation factor for a specific metal ion pair is chosen as the eluent. Consequently, an understanding of the eluents that can be employed for separation can be gained from a study on the distribution behavior of metal ions in several electrolyte media [28].

5.3.9.7. Binary and ternary separations of Ce-ATMP

This text's discussion of the high separation factor in a given medium has been applied to binary separations for the following metal ion pairs (under study): Ni^{2+} - Cu^{2+}, Zn^{2+} - Cu^{2+}, Co^{2+} - Cu^{2+}, Zn^{2+} - Ni^{2+}, Co^{2+} - Ni^{2+}, Co^{2+} - Zn^{2+}, Cd^{2+} - Pb^{2+}, Hg^{2+} - Pb^{2+}, Hg^{2+} - Cd^{2+} and Cd^{2+} - Pb^{2}. The separation effectiveness of transition metal ions in binary separations ranges from 70-91% while that of heavy metal ions is between 78-92%, **(Table 5.10)**. Symmetric bell-shaped curves also enable efficient separation **(Figures 5.28-5.30)**. The greatest percentage of metal eluted in all binary separation scenarios, regardless of the metal ion pair, Cu^{2+} < Ni^{2+} < Zn^{2+} < Co^{2+} amongst heavy metal ions and Pb^{2+} < Cd^{2+} < Hg^{2+} amongst transition metal ions. The separation factor (α) and the K_d values of metal ions are consistent with this finding. As previously mentioned, metal ions with high K_d values are less eluted, and vice versa. % of metal eluted reduces with declining separation factor and grows as you raise the separation factor [27,29].

The percentage of metal eluted in ternary separations for transition metal ions (Co^{2+} - Zn^{2+} - Cu^{2+}) and heavy metal ions (Hg^{2+} - Cd^{2+} - Pb^{2+}) ranges between 59-78% and 65-79%, respectively **(Table 5.10)**. There are three separate peaks in each case **(Figures 5.31 (a) and (b))**; nevertheless, the percentage of metal eluted is also fewer than in single and binary metal ion separations due to tailing effects for each metal ion eluted. The depletion of metal ions during eluent changeover, metal ion interference, pH, simultaneous elution of two or more metal ions with the same eluent, and, finally, experimental errors involved in the

determination of metal ions in the presence of other ions might be the causes of the separation process getting complex [29,20].

Table 5.10. Binary and Ternary Separations of Transition and Heavy metal ions utilizing Ce-ATMP.

Separations achieved	Eluent	Metal ion (mg)		Elution (%)
		Loaded (C_0)	Eluted (C_e)	
Co^{2+} - Cu^{2+}	(A) 0.2 M HNO_3 (Co^{2+})	0.5893	0.5421	91.99
	(B) 0.2 M $HClO_4$ (Cu^{2+})	0.6354	0.5250	82.65
Zn^{2+} - Cu^{2+}	(A) 0.2 M HNO_3 (Zn^{2+})	0.6538	0.5796	88.65
	(B) 0.2 M $HClO_4$ (Cu^{2+})	0.6354	0.5100	80.26
Ni^{2+} - Cu^{2+}	(A) 0.2 M HNO_3 (Ni^{2+})	0.5869	0.4935	84.08
	(B) 0.2 M $HClO_4$ (Cu^{2+})	0.6354	0.4950	77.90
Co^{2+} - Ni^{2+}	(A) 0.2 M HNO_3 (Co^{2+})	0.5893	0.5362	90.98
	(B) 0.2 M CH_3COOH (Ni^{2+})	0.5869	0.5020	85.53
Zn^{2+} - Ni^{2+}	(A) 0.2 M HNO_3 (Zn^{2+})	0.6538	0.5832	89.20
	(B) 0.2 M CH_3COOH (Ni^{2+})	0.5869	0.5006	85.30
Co^{2+} - Zn^{2+}	(A) 0.2 M HNO_3 (Co^{2+})	0.5893	0.5309	90.09
	(B) 0.2 M NH_4NO_3 (Zn^{2+})	0.6538	0.5865	89.71
Hg^{2+} - Pb^{2+}	(A) 0.2 M HNO_3 (Hg^{2+})	2.0059	1.8600	92.72
	(B) 0.2 M NH_4NO_3 (Pb^{2+})	2.0720	1.7168	82.26
Cd^{2+}- Pb^{2+}	(A) 0.2 M HNO_3 (Cd^{2+})	1.1241	0.9729	86.55
	(B) 0.2 M NH_4NO_3 (Pb^{2+})	2.0720	1.7423	84.09
Hg^{2+}- Cd^{2+}	(A) 0.2 M HNO_3 (Hg^{2+})	2.0059	1.8150	90.48
	(B) 0.2 M $HClO_4$ (Cd^{2+})	1.1241	0.9870	87.80
Co^{2+}- Zn^{2+}- Cu^{2+}	(A) 0.2 M HNO_3 (Co^{2+})	0.5893	0.4650	78.90
	(B) 0.2 M NH_4NO_3 (Zn^{2+})	0.6538	0.4690	71.73
	(C) 0.2 M $HClO_4$ (Cu^{2+})	0.6354	0.3870	60.90
Hg^{2+}- Cd^{2+}- Pb^{2+}	(A) 0.2 M HNO_3 (Hg^{2+})	2.0059	1.5900	79.26
	(B) 0.2 M $HClO_4$ (Cd^{2+})	1.1241	0.8260	73.48
	(C) 0.2 M NH_4NO_3 (Pb^{2+})	2.0720	1.3690	66.07

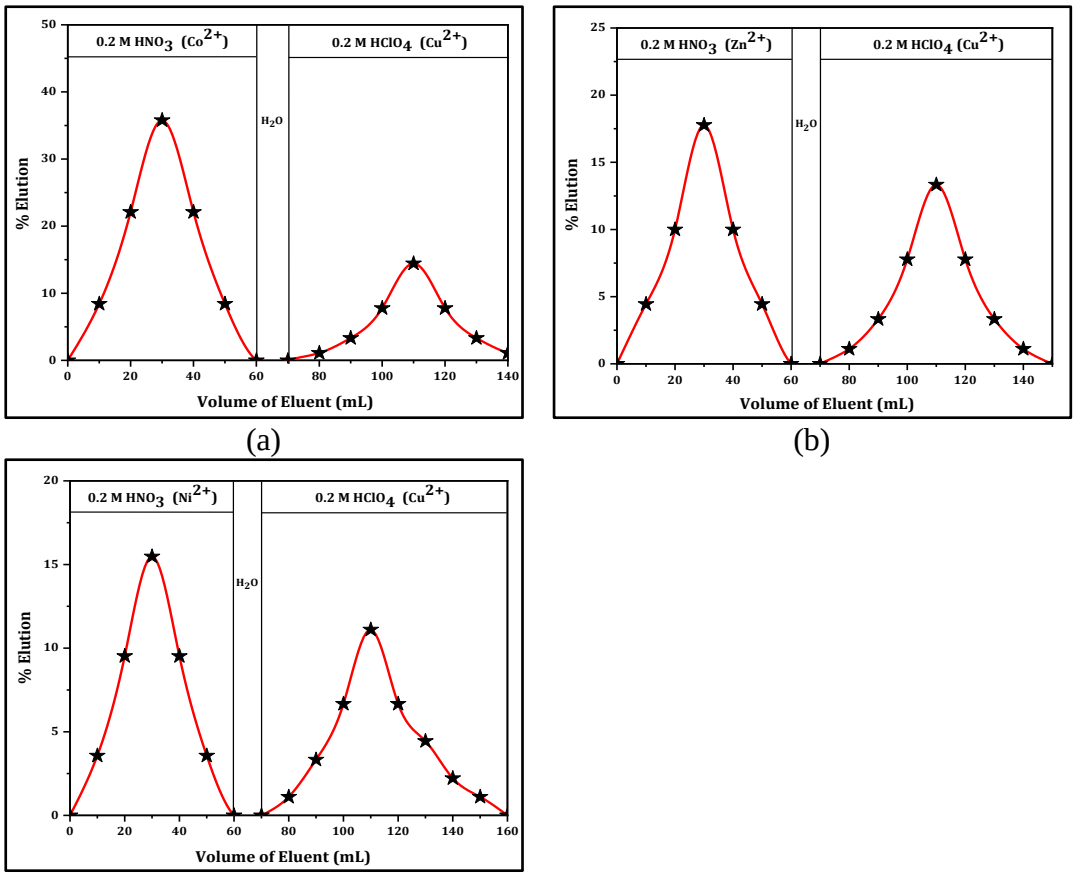

Figure 5.28. Binary separations of transition metal ions using Ce-ATMP: (a) Co^{2+}- Cu^{2+}, (b) Zn^{2+}- Cu^{2+}, (c) Ni^{2+}- Cu^{2+}.

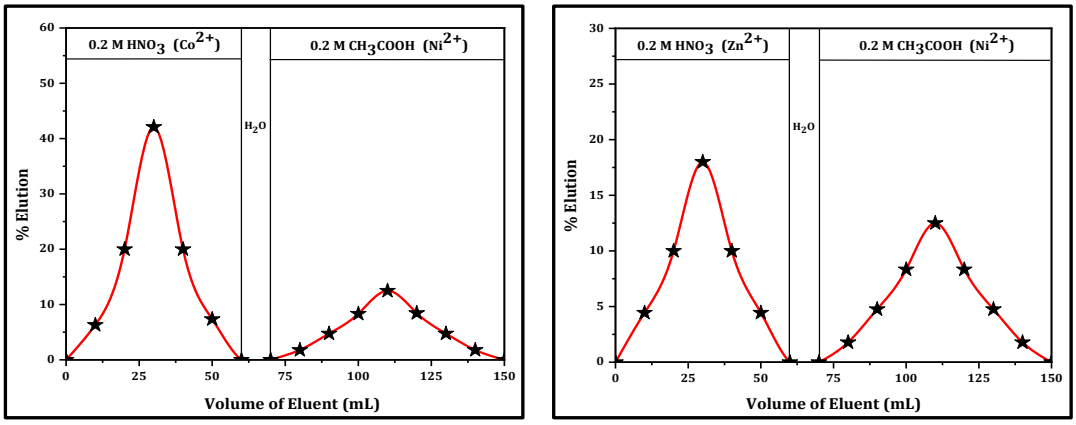

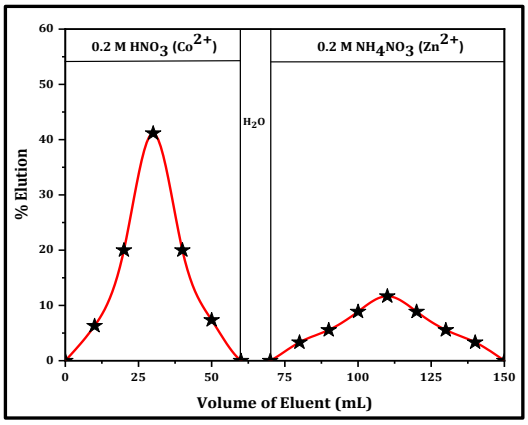

(c)

Figure 5.29. Binary separations of transition metal ions using Ce-ATMP: (a) Co^{2+}- Ni^{2+} (b) Zn^{2+}- Ni^{2+} (c) Co^{2+}- Zn^{2+}.

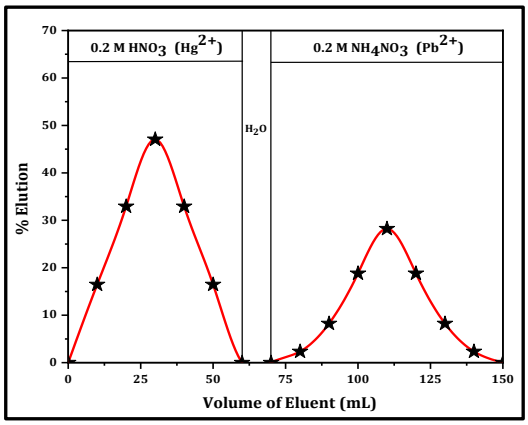

(a)

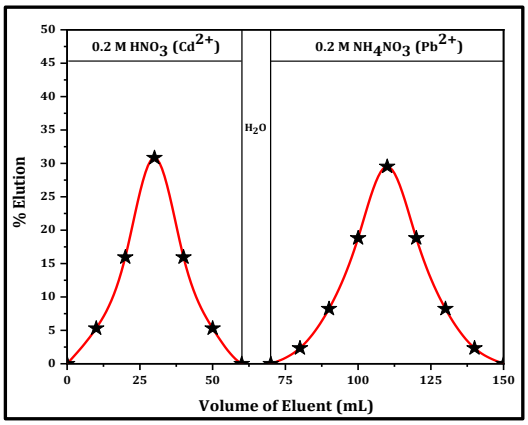

(b)

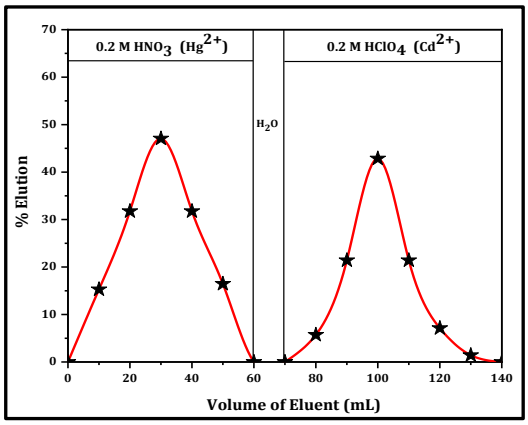

(c)

Figure 5.30. Binary separations of heavy metal ions using Ce-ATMP: (a) Hg^{2+}- Pb^{2+} (b) Cd^{2+}-Pb^{2+} (c) Hg^{2+}- Cd^{2+}.

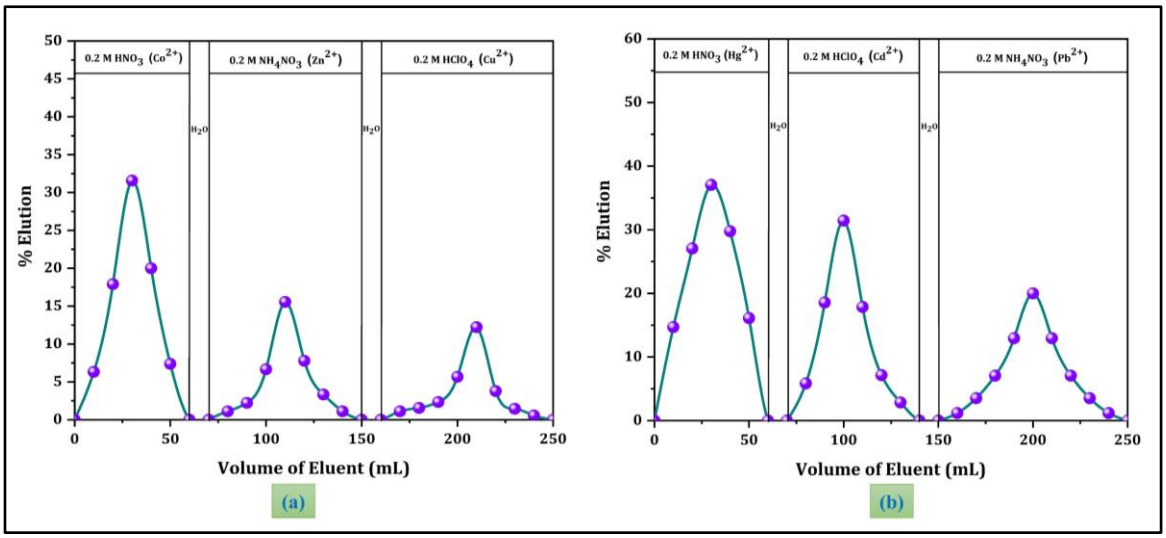

Figure 5.31. Ternary separations of transition and heavy metal ions using Ce-ATMP (a) Co^{2+}- Zn^{2+}- Cu^{2+} (b) Hg^{2+}- Cd^{2+}- Pb^{2+}.

5.3.9.8. Regeneration and reuse studies

After used, the exchanger can be restored to its initial state by using abundant nitric acid to eliminate the metal ions. **Figure 5.32**, shows plot of the percentage retention in K_d values against the number of cycles, indicates that Ce-ATMP may be regenerated and reused without significantly degrading performance. The percentage retention in K_d values were found to be nearly constant at ~100% up to four cycles [23,24].

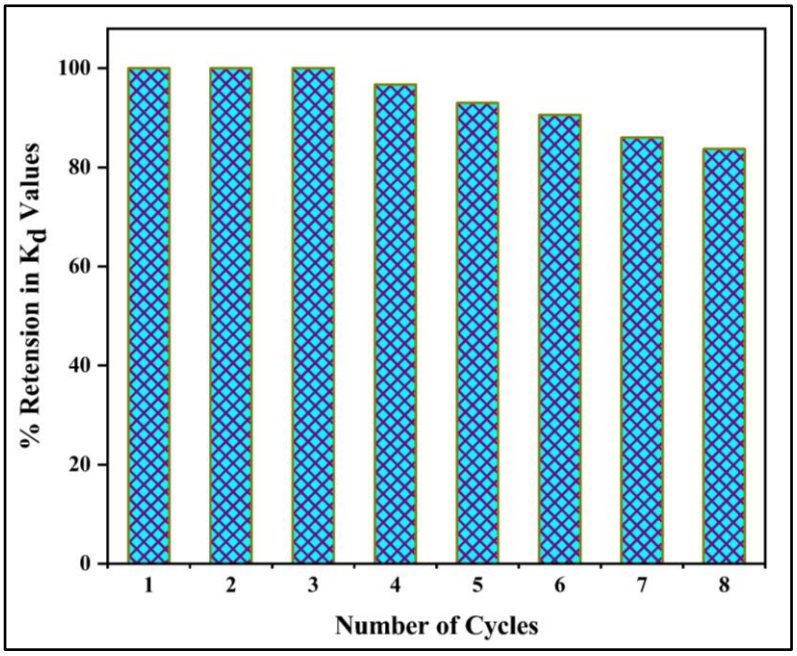

Figure 5.32. Plot of % retention in K_d value *versus* number of cycles using Ce-ATMP.

5.4. Conclusions

The physico-chemical and instrumental methods of analysis revel the promising ion-exchange properties of the prepared Ce-ATMP. Adsorption isotherm and thermodynamic parameters substantially support the observed a good metal ion affinity towards prepared Ce-ATMP for metal ions studied. The observed selectivity orders for the transition metal ions and heavy metal ions were as follows; $Cu^{2+} > Ni^{2+} > Zn^{2+} > Co^{2+}$ and $Pb^{2+} > Cd^{2+} > Hg^{2+}$ respectively. A high positive value of $\Delta H°$ implies endothermicity because of the greater dehydration of metal ions to occupy a site on the exchanger for which energy must be supplied; however, a higher negative value of $\Delta G°$ suggests feasibility and spontaneity of ion exchange process. The resin matrix experiences a high degree of disorder due to the ion exchange process, which is followed by a greater positive value of $\Delta S°$ was attributed to randomness. Hence, $\Delta G°$, $\Delta H°$, and $\Delta S°$ likewise corroborate the noted tendency. Kinetics studies indicate that the adsorption shows the best with pseudo-second-order kinetics. As results, Ce-ATMP possess a good potential can be utilized as a promising cation exchanger, as demonstrated by the effectiveness of its binary and ternary metal separation processes. Ce-ATMP was regenerated of various cycles without significantly degrading performance.

5.5. References

[1] Z. Fu, W. Guo, Z. Dang, Q. Hu, F. Wu, C. Feng, X. Zhao, W. Meng, B. Xing, J.P. Giesy. Environ. Sci. Technol. **51(6)** (2017) 3117–3118.

[2] Z. Tan, H. Peng, H. Liu, L. Wang, J. Chen, X. Lu, J. of App. Poly. Sci. **132(32)** (2015) 42384.

[3] M. Rafique, S. Hajra, M.B. Tahir, S.S.A. Gillani, M. Irshad, Environ. Sci. Pollut. Res. **29(11)** (2022) 16772–16781.

[4] D. Deng, M. Lamssali, N. Aryal, A. Ofori-Boadu, M.K. Jha, R.E. Samuel, Water Environ. Res. **92** (2020) 1805– 1810.

[5] A.L. Malik, A. Bashir, T. Manzoor, H.A. Pandith, RSC Advances **9(28)** (2019) 15976–15985.

[6] J.P. Chen, L.K. Wang, M.H.S. Wang, Y.T. Hung, N.K. Shammas, Remediation of Heavy Metals in the Environment; CRC Press, 2016.

[7] M. Boskabady, N. Marefati, T. Farkhondeh, F. Shakeri, A. Farshbaf, M.H. Boskabady, Environ. Int. **120** (2018) 404–420.

[8] L.A. Malik, A. Bashir, A. Qureashi, A.H. Pandith, Environ. Chem. Lett. **17(4)** (2019) 1495–1521.

[9] Mu. Naushad, G. Sharma, A. Kumar, S. Sharma, A.A. Ghfar, A. Bhatnagar, F.J. Stadler, M.R. Khan, Int. J. Biol. Macromol. **106** (2018) 1–10.

[10] A. Bashir, L.A. Malik, S. Ahad, T. Manzoor, M.A. Bhat, G.N. Dar, A.H. Pandith, Environ. Chem. Lett. **17(2)** (2019) 729–754.

[11] Y.P. Zhu, T.Y. Ma, Y.L. Liu, T.Z. Ren, Z.Y. Yuan, Inorg. Chem. Front. **1(5)** (2014) 360–383.

[12] A. Bashir, S. Ahad, L. A. Malik, A. Qureashi, T. Manzoor, G. N. Dar, A.H. Pandith, Ind. Eng. Chem. Res. **59(52)** (2020) 22353–22397.

[13] C. Kang, Y. Peng, Y. Tang, H. Huang, C. Zhong, Ind. Eng. Chem. Res. **56(46)** (2017) 13866–13873.

[14] S. Ghosh, P. Bhanja, N. Salam, R. Khatun, A. Bhaumik, Sk. M. Islam, Catal. Today **309** (2018) 253–262.

[15] T.Y. Ma, X.Z. Lin, X.J. Zhang, Z.Y. Yuan, New J. Chem. **34(6)** (2010) 1209–1216.

[16] Y. Cheng, G.K. Chuah, Chin. Chem. Lett. **31(2)** (2020) 307–310.

[17] C. Wang, X. Liu, N.K. Demir, J.P. Chen, K. Li, Chem. Soc. Rev. **45(18)** (2016) 5107–5134.

[18] I. Akhmetova, M. Rautenberg, C. Das, B. Bhattacharya, F. Emmerling, ACS Omega **8(19)** (2023) 16687–16693.

[19] T.F. Parangi, U.V. Chudasama, ACS Omega **4(2)** (2019) 3716–3725.

[20] P.R. Patel, U.V. Chudasama, Desalination Water Treat. **52(1–3)** (2014) 481–489.

[21] P. Bhanja, Y. Kim, K. Kani, B. Paul, T. Debnath, J. Lin, A. Bhaumik, Y. Yamauchi, Chem. Eng. J. **396** (2020) 125245.

[22] Q. Wang, C. Yang, Q. Yang, S. Yu, H. Yang, Anal. Chim. Acta **1046** (2019) 93–98.

[23] B. Shah, U. Chudasama, Sep. Sci. Technol. **54(10)** (2019) 1560–1572.

[24] B. Shah, U. Chudasama, Desalination Water Treat. **38(1–3)** (2012) 276–284.

[25] W. Mu, B. Chen, X. Nucl. Anal. **2(2)** (2023) 100072.

[26] R. Thakkar, U. Chudasama, J. Iran. Chem. Sci. **7(1)** (2010) 202–209.

[27] A.S. Jayswal, U.V. Chudasama, Asian J. Water Environ. Pollut. **6(1)** (2009) 97–101.

[28] R. Thakkar, U. Chudasama, J. Hazard. Mater. **172(1)** (2009) 129–137.

[29] P. Patel, U. Chudasama, Sep. Sci. Technol. **46** (2011) 1346−1357.

[30] A. Jayswal, U. Chudasama, Turk. J. Chem. **32(1)** (2008) 63–74.

[31] G.K. Akpomie, I.C. Ogbu, A.A. Osunkunle, M.A. Abuh, M.N. Abonyi, J. Emerg. Trends Eng. Appl. Sci. **3(2)** (2012) 354–358.

[32] A.E. Kurtoğlu, G. Atun, Sep. Purif. Technol. **50(1)** (2006) 62–70.

[33] S. Sinha, S.S. Behera, S. Das, A. Basu, R.K. Mohapatra, B.M. Murmu, N.K. Dhal, S.K. Tripathy, P.K. Parhi, Chem. Eng. Commun. **205(4)** (2018) 432–444.

[34] I.M. Ali, M.Y. Nassar, Y.H. Kotp, M. Khalil, Part. Sci. Technol. **37(2)** (2019) 207–219.

[35] P. Patel, U. Chudasama, Ion Exch. Lett. **4(2)** (2011) 7–15.